

# **Developing a conceptual sizing tool for eVTOL by OpenConcept**

**Student  
Po-Chih Chou**

**Advisor  
Joaquim R. R. A. Martins**



**Aerospace Engineering  
University of Michigan, Ann Arbor  
United States  
April, 21, 2021**

# Contents

<b>1 Abstract . . . . .</b>	<b>3</b>
<b>2 Reviewing works in 2021 Fall Semester . . . . .</b>	<b>3</b>
<b>3 Goals and work done in 2022 winter Semester . . . . .</b>	<b>3</b>
<b>4 Introduction . . . . .</b>	<b>4</b>
<b>5 eVTOL Weight and Propulsion Modeling . . . . .</b>	<b>4</b>
5.1 Weight Estimation . . . . .	4
5.2 Flight Mission Analysis Model . . . . .	7
5.3 Static Stability . . . . .	14
<b>6 OEW Model Validation . . . . .</b>	<b>16</b>
6.1 Existing Multi-Rotor eVTOL . . . . .	16
6.2 Existing Tilt-Wing eVTOL . . . . .	18
6.3 Existing Tilt-Rotor eVTOL . . . . .	20
<b>7 Reproduce Literature Flight Mission . . . . .</b>	<b>21</b>
<b>8 Multidisciplinary Design Optimization Study . . . . .</b>	<b>24</b>
8.1 Optimizing Literature case for On-demand Mission Requirement . . . . .	25
8.2 MTOW minimization . . . . .	29
8.3 Extreme Range Study Across eVTOL Configurations . . . . .	34
<b>9 Summary . . . . .</b>	<b>37</b>
<b>10 Future Work . . . . .</b>	<b>38</b>
<b>Appendices . . . . .</b>	<b>41</b>
<b>A Analysis Benchmarking . . . . .</b>	<b>41</b>
A.1 Problem Formulation . . . . .	41
A.2 Results and Discussion . . . . .	41

# List of Figures

1 Propeller weight regression model(produced from [1]) . . . . .	5
2 Flow model for momentum theory in axial climbing flight . . . . .	7
3 Propeller efficiency map for the case study (national; not to be used for industry study) [2] . . . . .	9
4 Momentum analysis of a rotor in forward flight . . . . .	11
5 Flow model for a coaxial analysis . . . . .	13
6 A demonstration of a propulsion layout with a 6-rotor eVTOL . . . . .	14
7 Force and moments for longitudinal trim and static stability; arrows show positive quantities. Note that $M_w$ and $L_h$ are usually negative. . . . .	14
8 Existing multi-rotor eVTOL, EHang 184 and EHang 216 . . . . .	17
9 Existing multi-rotor eVTOL, CityAirbus and Volocopter 2X . . . . .	17
10 Dimension of Airbus A <sup>3</sup> Vahana . . . . .	20
12 Figures for the mission validation . . . . .	22
13 Mission analysis validation result plots . . . . .	24
14 Mission profile of MDO validation . . . . .	26
15 Mission analysis validation result plots . . . . .	27
16 Aircraft weights ratio of MTOW minimization . . . . .	31

17	Component weights ratio of MTOW minimization . . . . .	32
18	Tilt-rotor cruise drag . . . . .	34
19	Aircraft weights and MTOW ratio results of extreme range studies . . . . .	36
20	Aircraft Component weights and MTOW ratio results of extreme range studies	37
21	MTOW converge history . . . . .	42

## List of Tables

1	Equivalent skin friction coefficient . . . . .	10
2	Variables in Eqn. 46 . . . . .	15
3	Existing eVTOL vehicle specifications [3][4] . . . . .	18
4	Comparison between published and modeled results for existing multi-rotor eVTOL . . . . .	18
5	Existing tilt-wing eVTOL vehicle specifications [5] . . . . .	19
6	Existing tilt-wing vehicle calculated OEW . . . . .	19
7	Existing tilt-rotor vehicle specifications [6][7] . . . . .	21
8	Comparison between published and modeled results for existing tilt-rotor eVTOL . . . . .	21
9	Mission profile validation for tilt-rotor vehicle . . . . .	22
10	Comparison and sizing validation for a tilt-rotor eVTOL . . . . .	23
11	Mission profile optimization validation . . . . .	25
12	Tilt-rotor setup for on-demand validation . . . . .	28
13	On-demand mission requirement optimization result . . . . .	28
14	MTOW minimization problem for EHang 216-class vehicle . . . . .	29
15	MTOW minimization problem for CityAirbus-class vehicle . . . . .	30
16	MTOW minimization problem for JobyS4-class vehicle . . . . .	30
17	Optimizer Benchmark . . . . .	41

## 1 Abstract

Research on the new eVTOL marketing has dramatically expanded in the last decades, presenting a new need in crowded city areas. Many startups have developed their product in the past ten years. Unlike conventional aircraft, these data are usually inaccessible to these startups. A conceptual design and optimization tool for eVTOL is presented in this report. The tool is built on the OpenConcept, an open-source aircraft conceptual design tool written on NASA's OpenMDAO framework. This tool enables users to create their vehicle model by specifying eVTOL specifications in dimension, propulsion layout, and mission profiles for further analysis. The weight and propulsion payout of each eVTOL are estimated from different resources for different eVTOL configurations. Also, the maximum rotor speed is considered for noise consideration for all models during all mission segments. Three Multidisciplinary Design Optimization (MDO) studies are provided in this report: one on the optimization validation with other literature; one on minimizing the maximum takeoff weight (MTOW); one on exploring the extreme condition for eVTOL; and one on the optimizer benchmark. The optimization results show a significant trend from what we expected for the electrical aircraft. The results give insight into different component weights-to-MTOW for each payload and cruise speed case. More, the aerodynamics model and battery weight ratio are critical factors in the MDO study. Last, some future works were provided.

## 2 Reviewing works in 2021 Fall Semester

In the previous semester, 2020 fall, this report studied the weight estimation and mission analysis of a tilt-rotor eVTOL with six rotors. In this report, the empty weight validations with different configurations of vehicles were conducted. They showed an error of 32%, 1.2%, and 12% for multi-rotor (EHang 216), tilt-wing (Airbus A<sup>3</sup> Vahabna  $\beta$ ), and tilt-rotor (Joby S4) configuration, respectively. The mission validation was also performed by comparing with [8]. In addition, the multidisciplinary design optimization for a tilt-rotor configuration was studied, and proposed trends and weight composition within the cruise range of 30 miles and cruise speed of 150 miles per hour. However, the propulsion model needs further improvement in the report since we modeled the vertical flight phase by implementing the propeller designed for high-speed cruise flight. Mortification of the propulsion is necessary for future works.

## 3 Goals and work done in 2022 winter Semester

The first task this semester is to refine the propulsion model. This report implemented the momentum theories in the vertical takeoff and landing phase while maintaining the same analysis methodology in the cruise phase for a tilt-rotor configuration. Also, the new multi-rotor configuration was introduced, and the corresponding propulsion model during level cruise flight was also added to this report. The coaxial rotor system and new rotor weight model were introduced to capture the existing players better. Finally, for the multidisciplinary design optimization study, two models, MDO validation and minimizing MTOW, were refined; two new models, optimizer benchmarking and extreme study, were added.

## 4 Introduction

The OpenConcept, the OpenMDAO-based toolkit for conceptual aircraft, is used for this report. This toolkit was developed to model and optimize aircraft with electric propulsion at low computation cost and allowed users to define over a hundred needed variables when doing the aircraft conceptual design. There are already some examples given in the OpenConcept by [9], such as Boeing 737, TBM 50, Caravan, and King Air C90 GT. They all have well-defined flight data, aircraft models, and the complete mission analysis model. However, this tool kit is not for high fidelity design purposes. One of these purposes is the fidelity of CFD analysis during any mission segment. Users either define their model for the aerodynamics characteristics during the flight mission or pre-defined variables that they are interested in before running any analysis.

Based on the OpenConcept, we are developing a similar methodology for the eVTOL/Urban Air Mobility (UAM) conceptual design. Many things differ from conventional small or hybrid aircraft. The weighted model and the flight mission segment are the most prominent components. More, since there is seldom data that the current eVTOL industry has released, many aircraft models are estimated in this report.

Section 5 presents methodologies we use to eVTOL conceptual design, and we do the weight model validation in section 6, which end up showing that a great weight match with the existing eVTOL models. 7 performs a weight, mission, and optimized model validation with Duffy [10] literature, which is a valuable result for developing our eVTOL conceptual toolkit. Finally, we perform a series of multidisciplinary design optimization in section 8. The results discuss the maximum takeoff weight (MTOW) relation with cruise velocity, cruise range, and battery energy density. Lastly, 10 9 summarized this report and provided guidelines and thoughts for future development from this report.

## 5 eVTOL Weight and Propulsion Modeling

The first step of developing an aircraft model based on the OpenConcept frame is to create a weight estimation model. The data and the weight regression model are collected from verities of aircraft, helicopters design textbooks, and some literature. For example, we used the Cessna methods in the wing components and the helicopter model for equipment weight.

### 5.1 Weight Estimation

The empty is composed of three major segments for an aircraft. Therefore, we use a similar approach in developing our eVTOL model. The model needed for estimating the empty operation weight is provided by the (1).

First, the Operating Empty weight (OEW) can be broken into the following groups,

$$\text{OEW} = W_{\text{empty}} = W_{\text{frame}} + W_{\text{propulsion}} + W_{\text{equipment}} \quad (1)$$

#### 5.1.1 Airframe Weights, $W_{\text{frame}}$

The airframe weights of an eVTOL can be further expressed into,

$$W_{\text{frame}} = W_{\text{fuselage}} + W_{\text{wing}} + W_{\text{empennage}} + W_{\text{landing gear}} \quad (2)$$

The fuselage weight is estimated from the helicopter model Ref. [11].

$$W_{\text{fuselage}} = 6.9 \left( \frac{\text{MTOW}}{1000} \right)^{0.49} L_{\text{fuselage}}^{0.61} (S_{\text{wet, fuselage}})^{0.25} \quad (3)$$

where MTOW is the maximum takeoff weight (lb),  $L_{\text{fuselage}}$  is the fuselage length (ft), and the  $S_{\text{wet, fuselage}}$  is the fuselage wetted area in ( $\text{ft}^2$ ).

The wing weight is measured from the Cessna-like small aircraft from Ref. [12].

$$W_{\text{wing}} = 0.04674 \text{MTOW}^{0.397} S_{\text{wing}}^{0.360} n_{\text{ult}}^{0.397} AR^{1.172} \quad (4)$$

where  $S_{\text{wing}}$  is the reference wing area ( $\text{ft}^2$ ),  $n_{\text{ult}} = 3$  is the ultimate load factor, and AR is the wing aspect ratio.

The empennage weight is modeled from Torenbeek methods in the Ref. [12],

$$W_{\text{empennage}} = 0.04 (n_{\text{ult}} (S_{\text{ref,vert}} + S_{\text{ref,horiz}}))^2^{0.75} \quad (5)$$

where  $S_{\text{ref,vert}}$  and  $S_{\text{ref,horiz}}$  are the referencing areas of the vertical and horizontal stabilizer in ( $\text{ft}^2$ ).

The landing gears weight is modeled from Prouty, Ref.[11],

$$W_{\text{landing gear}} = \frac{40}{1000^{0.67}} \text{MTOW}^{0.67} 3^{0.54} \quad (6)$$

### 5.1.2 eVTOL Propulsion group weights, $W_{\text{propulsion}}$

Then we break down the propulsion group weights as following,  $W_{\text{propulsion}}$  includes,

$$W_{\text{propulsion}} = W_{\text{rotors and hubs}} + W_{\text{motors}} + W_{\text{nacelle}} + W_{\text{motor controller}} \quad (7)$$

The prop weight is modeled from regression of the current single turboprop propeller manufacturer and provider, Ref

$$W_{\text{prop}} = 0.003 \phi^{2.8094} N_{\text{props}} \quad (8)$$

where  $\phi$  is the propeller diameter (inch), and  $N_{\text{props}}$  is the number of the propellers. Figure 1 provides a propeller regression model form manufacturer data [1].

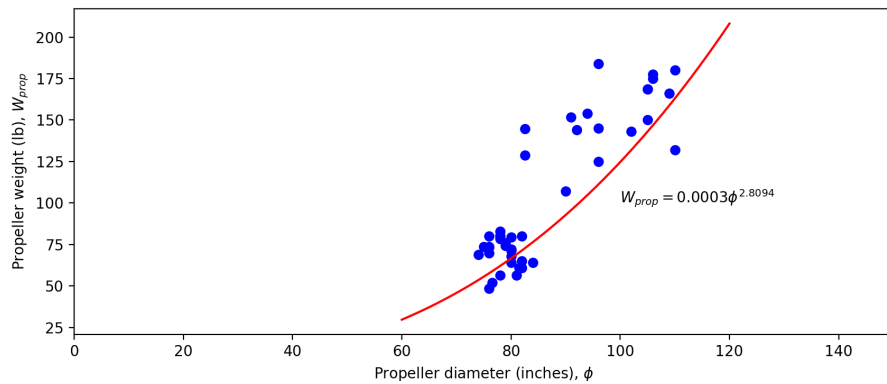


Figure 1: Propeller weight regression model (produced from [1])

if the eVTOL used the rotor instead of propeller, the rotor weight can be found as,

$$W_{\text{rotor}} = 0.026N_b^{0.66}b_c(\phi/(2*12))1.3V_{\text{tip}}^{0.67}N_{\text{props}} \quad (9)$$

where  $N_b$  is the number of blades,  $b_c$  is the blade chord length [inch],  $\phi$  is the rotor diameter [inch],  $V_{\text{tip}}$  is the blade tip speed [ft/s],  $N_{\text{props}}$  is the number of rotor.

The motor weight is measured as,

$$W_{\text{motor}} = \rho_{\text{motor}}P_{\text{TO}}N_{\text{motors}} \quad (10)$$

where  $\rho_{\text{motor}}$  is the motor power density in (kW/kg),  $P_{\text{TO}}$  is the power required for hover in (kW), and  $N_{\text{motors}}$  is the number of motors. The motor power density as 5 (kW/kg) in this case.

The nacelle weight is modeled from Roskam method, Ref. [12],

$$W_{\text{nacelle}} = 0.14P_{\text{TO}}N_{\text{props}} \quad (11)$$

where  $P_{\text{TO}}$  is the power required for hover in (kW).

Finally, the motor controller weights are estimated from Kadhiresan and Duffy [8],

$$W_{\text{motor controller}} = 2.20462(0.12537(P_{\text{TO}} - 2) + 0.1)N_{\text{props}} \quad (12)$$

where  $P_{\text{TO}}$  is the power required for takeoff in (kW).

### 5.1.3 eVTOL Equipment weights, $W_{\text{equipment}}$

The following equipment are considered for every eVTOL model. The equipment weight is given by,

$$W_{\text{equipment}} = W_{\text{flight control}} + W_{\text{avionics}} + W_{\text{ac}} + W_{\text{instruments}} + W_{\text{fur}} + W_{\text{paint}} \quad (13)$$

The flight control system weight is,

$$W_{\text{flight control}} = 0.23\text{MTOW}^{0.66} \quad (14)$$

where MTOW in is the maximum takeoff weight in (lb).

From Prouty, Ref.[11], avionics are guessed as,

$$W_{\text{avionics}} = 50(\text{lb}) \quad (15)$$

The air condition weight is modeled as following by Prouty, Ref.[11],

$$W_{\text{ac}} = 8\frac{\text{MTOW}}{1000} \quad (16)$$

where MTOW is the maximum takeoff weight in (lb).

The instrument weight is estimated from Prouty, Ref.[11],

$$W_{\text{instruments}} = 3.5\frac{\text{MTOW}^{1.3}}{1000} \quad (17)$$

MTOW is maximum takeoff weight in (lb).

The furnishing weights like seat and decorations are estimated by Prouty, Ref.[11],

$$W_{\text{fur}} = 0.412N_{\text{pax}}^{1.145} \text{MTOW}^{0.489} \quad (18)$$

where  $N_{\text{pax}}$  is the number of passengers, and MTOW is the maximum takeoff weight in (lb).

Lastly, the painting weight is again estimated by Prouty, Ref.[11],

$$W_{\text{paint}} = 0.003\text{MTOW} \quad (19)$$

The  $MTOW$  is the maximum takeoff weight in (lb).

## 5.2 Flight Mission Analysis Model

### 5.2.1 Vertical takeoff and landing phase

In the vertical takeoff and landing phase, the steady condition of the momentum theory is considered.

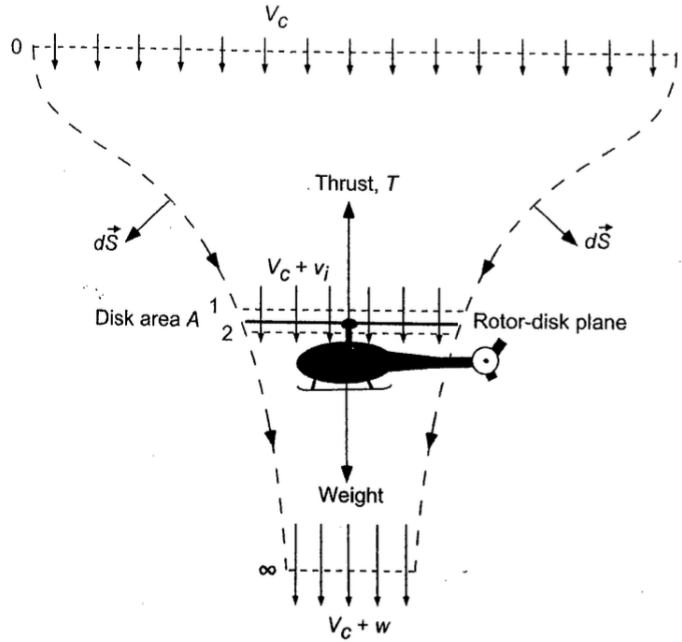


Figure 2: Flow model for momentum theory in axial climbing flight

To determine the power need for takeoff and landing phase, we first need to know the disk load (D.L.)

$$D.L. = \sqrt{\frac{T}{2\rho A}} \quad (20)$$

where  $T$  is the thrust (lb) of one motor, which is the ratio of MTOW and the number of rotor in the vertical motion, the drag force during the vertical motion has been ignored. From the momentum theory, the ideal power needed to lift the aircraft is described as,

$$P_{\text{hover}}(\text{h.p.}) = T \frac{\sqrt{D.L.}}{38F.M.} \quad (21)$$

in our case, the ideal hover power is therefore,

$$P_{\text{hover}}(\text{h.p.}) = \frac{T}{N_{\text{rotor}}} \frac{\sqrt{D.L.}}{38F.M.} \quad (22)$$

where T is the thrust (lb), D.L. is disk load in ( $\text{lb}/\text{ft}^2$ ), F.M. = 0.8 is Figure of Merit,  $P_{\text{hover}}$  is the ideal hover power in (h.p.). To know the power required for a given climb rate, the ideal hover induce velocity needs to be determined. Therefore, the induce velocity,

$$V_h(\text{ft/s}) = \sqrt{\frac{MTOW/N_{\text{rotor}}}{2\rho A}} \quad (23)$$

where  $\rho$  is the air density in ( $\text{slug}/\text{ft}^3$ ), A is the rotor disk area. Before calculating the climb and descend power for a given climb/descend rate, the vortex ring state  $-2 < V_{\text{vertical}}/V_h < 0$ , where the momentum theory fails, needs to be considered. The velocity ratio is used to determine whether the descend phase is in a vortex ring state or not, and the corresponding power model can be implemented. From the momentum theory, the power ratio  $P/P_h$  between power required  $P$  and hover  $P_h$  for the vertical motion can be defined as following,

$$\frac{P}{P_h} = \begin{cases} \frac{V_C}{2v_h} + \sqrt{(\frac{V_C}{2v_h})^2 + 1} & , \frac{V_C}{2v_h} \geq 0 \\ \frac{V_D}{2v_h} - \sqrt{(\frac{V_D}{2v_h})^2 - 1} & , \frac{V_C}{2v_h} \leq -2 \end{cases} \quad (24)$$

where  $P$  and  $P_h$  are both in hp,  $V_C$  is the climb rate in ft/s,  $v_h$  is the rotor induced velocity in ft/s. It is worth to notice that both  $V_C$  and  $v_h$  must be positive numbers since the velocity direction defined in the momentum theory. In the same fashion, the  $V_C$  must be negative to fulfill the sign consistency in the momentum theory. The region where the momentum region is invalid is usually called the vortex ring region. The power required from this region can be expressed as follows,

$$\frac{P}{P_h} = 0.974 - 0.125\left(\frac{V_D}{2v_h}\right) - 1.732\left(\frac{V_D}{2v_h}\right)^2 - 1.728\left(\frac{V_D}{2v_h}\right)^3 - 0.665\left(\frac{V_D}{2v_h}\right)^4 \quad (25)$$

### 5.2.2 Cruise

### 5.2.3 Power required for vertical cruise for the Winged Configuration

The equation of motions used in these three phases is again assumed as a steady-state of motions, where an winged eVTOL has no vertical and horizontal accelerations during cruise phase. The motion equation can be expressed as,

$$\begin{aligned} T \cos(\theta) &= D + W \sin(\gamma) \\ T \sin(\theta) &= \mathcal{L} + W \cos(\gamma) \end{aligned} \quad (26)$$

the  $T$  is the thrust and is set automatically to ensure a steady flight,  $\theta$  is the rotor angle with respect to the flight path in deg,  $\gamma$  is the flight path angle with respect to the global ground (horizontal plane),  $W$  is the vehicle weight,  $D$  and  $\mathcal{L}$  are the total drag and lift force produced

in each analysis node of the cruise phase. In the cruise phase, the absolute airspeed, vertical speed, cruise duration, and rotor angle  $\theta$  are defined by the user. The drag in the steady flight phase is estimated from the OpenConcept aerodynamics PolarDrag by Brelje [9]. While the lift force generated by the wing is calculated as follows,

$$\mathcal{L} = qS_{\text{ref,wing}}C_{\text{L, current flight condition}} \quad (27)$$

An winged eVTOL model equips an constant-speed propeller, the propeller is modeled from the online data [2] and is summerized by Brelje [13].

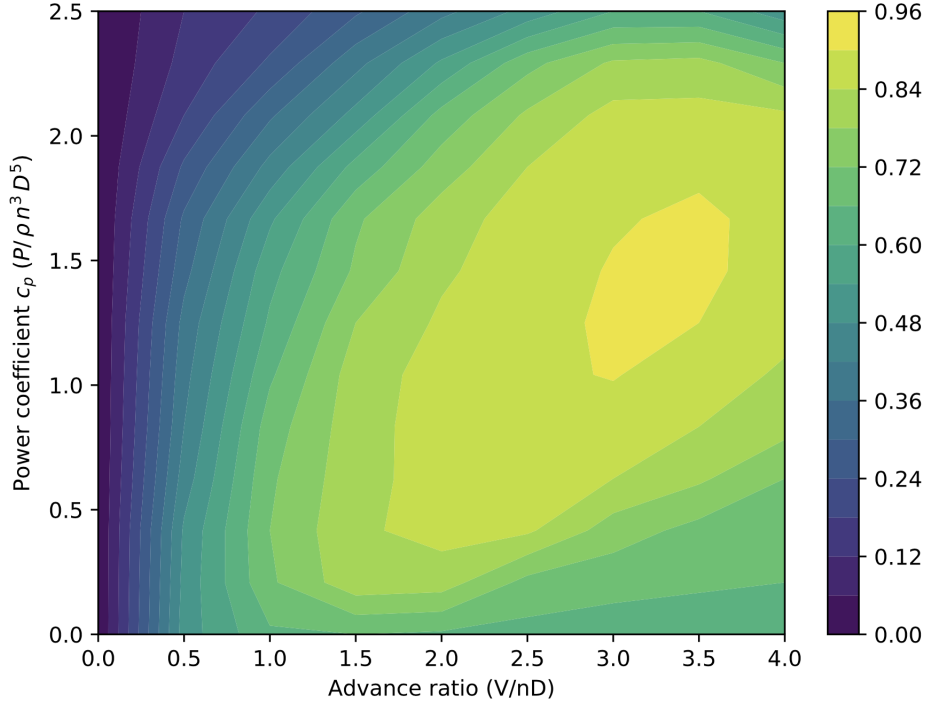


Figure 3: Propeller efficiency map for the case study (national; not to be used for industry study) [2]

The Cruise Drag,  $D$ , is defined by drag polar,

$$D = qS_{\text{ref}}(C_{D0} + \frac{C_L^2}{\pi A Re}) \quad (28)$$

where  $q$  is the dynamics pressure,  $S_{\text{ref}}$  is the wing reference area,  $C_{D0}$  is the parasite drag coefficient, and  $e$  is the Oswald efficiency factor = 0.8 during cruise, clean configuration. The Parasite drag coefficient can be written as,

$$C_{D0} = \frac{f}{S} \quad (29)$$

where  $f$  is the equivalent parasite area, which is proportional to the wetted area, i.e.,

$$f = C_f S_{\text{wet}} [\text{ft}^2] \quad (30)$$

The wetted area can be recovered from the historical date since lacking drawing of the aircraft. That is,

$$S_{\text{wet}} = 10^c W_0^d \text{ [ft}^2\text{]} \quad (31)$$

where  $c = 0.08635$  and  $d = 0.5632$  are configuration dependent regression constants. From the equivalent skin friction coefficient,

Table 1: Equivalent skin friction coefficient

	$C_f$
Bomber	0.0030
Civil transport	0.0026
Military cargo (high upsweep fuselage)	0.0035
Air Force Fighter	0.0035
Navy Fighter	0.0040
Light aircraft - single engine	0.0055
Light aircraft - twin engine	0.0045
Prop seaplane	0.0065
Jet seaplane	0.0045

We chose the  $C_f = 0.0030$  for somewhere between the civil aircraft and twin engine light aircraft.

#### 5.2.4 Power required for vertical cruise for the Multi-Rotor

Since the nature of the multi-rotor eVOTL, the lift force was not generated by the wing, the new model during the cruise flight is required. From Leishman[14], the treatment of rotor performance in forwarding flight was first derived by Glauert. Moreover, the Glauert model is shown, where the analysis is performed on an axis aligned with a rotor disk.

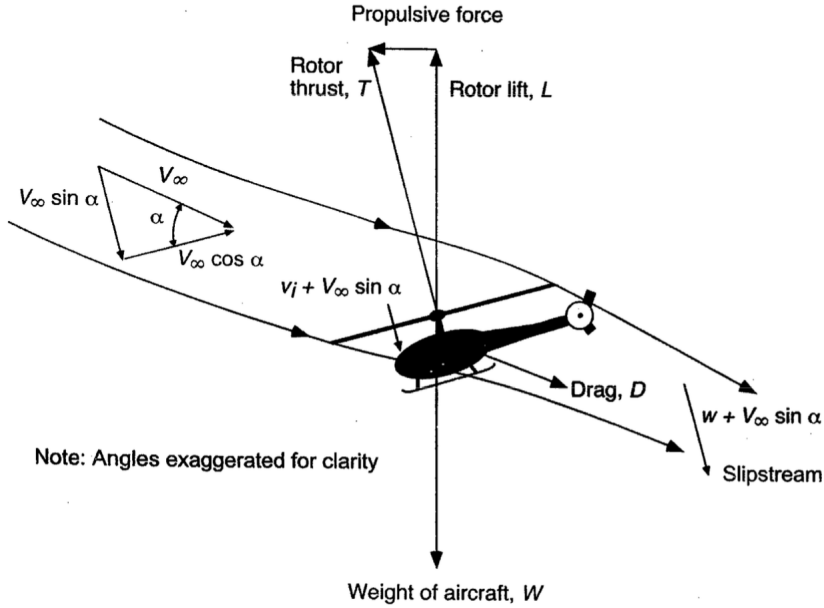


Figure 4: Momentum analysis of a rotor in forward flight

From the momentum theory, the thrust required in the forward flight is given by,

$$T = 2mv_i = 2(\rho AU)v_i \quad (32)$$

or

$$T = 2\rho A v_i \sqrt{(V_\infty \cos \alpha)^2 + (V_\infty \sin \alpha + v_i)^2} \quad (33)$$

where  $T$  is the single rotor thrust,  $v_i$  is the rotor induced velocity, and  $\alpha$  is the rotor angle of attack. And therefore, the induced velocity in forwarding flight can be written as

$$v_i = \frac{v_h^2}{\sqrt{(V_\infty \cos \alpha)^2 + (V_\infty \sin \alpha + v_i)^2}} \quad (34)$$

the idea of a tip speed ratio or advance ratio is now used. By using the velocity parallel to the plane of the rotor, we define  $\mu = V_\infty \cos \alpha / \Omega R$ . The inflow ration is  $\lambda = (V_\infty \sin \alpha + v_i) / \Omega R$ . This leads to the expression,

$$\lambda = \frac{V_\infty \sin \alpha}{\Omega R} + \frac{v_i}{\Omega R} = \mu \tan \alpha + \lambda_i \quad (35)$$

where  $\Omega R$  is the tip speed[ft/s]. From Eqn.[34],

$$\lambda_i = \frac{\lambda_h^2}{\sqrt{\mu^2 + \lambda^2}} \quad (36)$$

also, we know the relation between thrust coefficient and hover inflow ratio.

$$\lambda_i = \frac{C_T}{2\sqrt{\mu^2 + \lambda^2}} \quad (37)$$

Finally, the inflow ratio,

$$\lambda = \mu \tan\alpha + \frac{C_T}{2\sqrt{\mu^2 + \lambda^2}} \quad (38)$$

In this report, the methods from the OpenMDAO package, `om.ImplicitComponent` was implemented along with the nonlinear Newton solver and direct linear solver to find the corresponding inflow rate. By knowing the inflow rate, the momentum theory can be used for obtaining the power required for the forward flight as a ratio to the hover power, which was determined in the vertical segment by the following equation,

$$\frac{P}{P_h} = \frac{P}{Tv_h} = \frac{T(V_\infty \sin\alpha + v_i)}{Tv_h} = \frac{V_\infty \sin\alpha + v_i}{v_h} = \frac{\lambda}{\lambda_h} \quad (39)$$

From the drag model, by assuming the straight-and-level flight the disk angle of attack,  $\alpha$ , can be calculated from a simple force equilibrium. For vertical equilibrium  $T = \cos\alpha = W$  and for horizontal equilibrium  $T \sin\alpha = D \cos\alpha \approx D$ , Therefore,

$$\tan \alpha = \frac{D}{W} = \frac{D}{L} \approx \frac{D}{T} \quad (40)$$

### 5.2.5 Coaxial rotor systems

In this report, we introduced the coaxial rotor system to simulate the existing multi-rotor model. To simplify the process, the fixed Figure of Merit was used, and the fully developed slipstream from the upper rotor was considered.

From Leishman[14], The power for the upper rotor is  $P_u = Tv_u = Tv_h$  and for the lower rotor  $P_l = T(v_u + v_i) = 1.5616Tv_h$ . Therefore, for both rotors the total power is  $2.5616Tv_h$ , which is larger than two isolated rotors of  $2T$ . By introducing the induced power factor,  $\kappa_{int}$ ,

$$\kappa_{int} = \frac{(P_i)_{coax}}{(2P_i)_{isolated}} = \frac{2.5616Tv_h}{2Tv_h} = 1.281 \quad (41)$$

when the coaxial is operated at equal torque,

$$\kappa_{int} = \frac{2P_u}{(T_u + T_l)v_u} = 1.281 \quad (42)$$

Since we were assuming the same torque output for two rotors in a coaxial system for all models in this report, the required power for a coaxial system was assumed as  $1.281(2P_i)_{isolated}$ , and the lower rotor is considered to operate in the fully developed slipstream of the upper rotor.

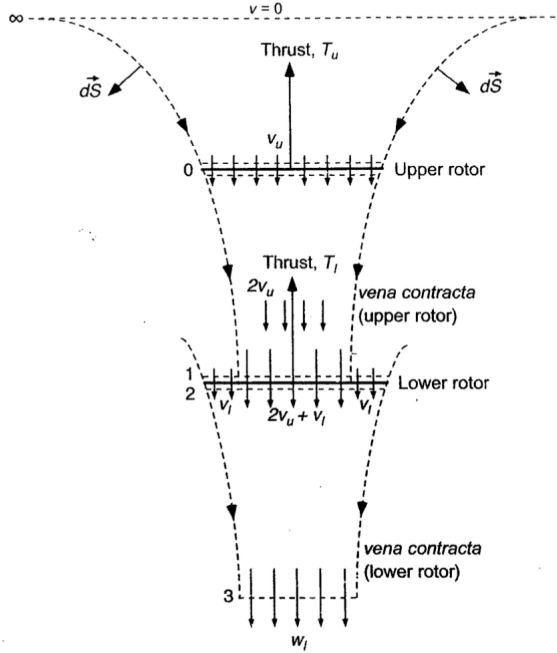


Figure 5: Flow model for a coaxial analysis

### 5.2.6 Tip speed and noise consideration

From Brown [15], the rotor Mach number was limited to 0.55 for the further multidisciplinary design optimization studies in this report. Therefore, the maximum propeller/ rotor rpm was subjected to,

$$V_{tip,max} = Ma = \pi\phi RPM_{max} \quad (43)$$

where  $V_{tip,max}$  is the maximum tip speed [m/s], M is the Mach number, a is the speed of sound [m/s],  $\phi$  is the propeller/ rotor diameter (m),  $RPM_{max}$  is the maximum propeller/ rotor RPM. And from speed of sound,

$$\alpha = \sqrt{\gamma RT} \quad (44)$$

where  $\gamma$  is the heat capacity ratio of air, R is the gas constant [287J/mol·K], and T is the local temperature[K].

### 5.2.7 Propulsion model

The propulsion layout used in this report is shown in Fig. 6. Each motor in the propulsion model rotates at the same rpm and generates the same thrust. The total thrust generated is obtained by adding the thrust produced together from each motor. In the same fashion, the propmodel adds every energy from each motor to calculate the energy consumption.

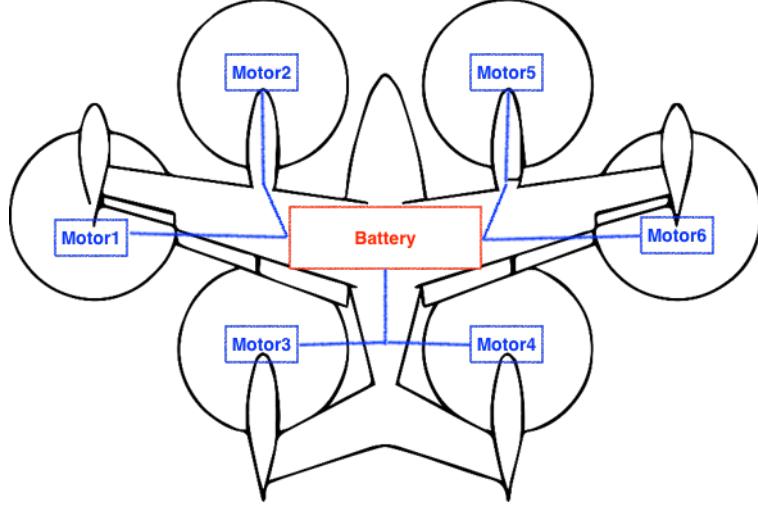


Figure 6: A demonstration of a propulsion layout with a 6-rotor eVTOL

Based on the equation of motion in each phase, the throttle is set automatically to ensure the steady flight. The **shaft power output** can be calculated by,

$$P_{\text{output}} = P_{\text{design}}(\text{throttle}) \quad (45)$$

$$0 \leq \text{throttle} \leq 1.2$$

$P_{\text{output}}$  and  $P_{\text{design}}$  are the power consumption and motor power rating in [kW], **throttle** is the throttle state (between 0 to 1.2) calculated automatically from the motion of equation in each mission separated mission segment.

### 5.3 Static Stability

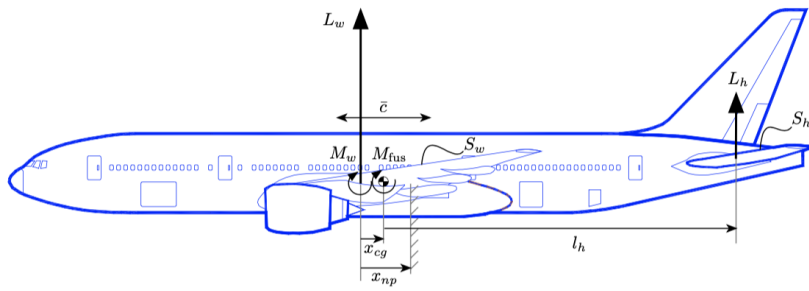


Figure 7: Force and moments for longitudinal trim and static stability; arrows show positive quantities. Note that  $M_w$  and  $L_h$  are usually negative.

The analysis of longitudinal stability and trim begins with expression for the pitching moment about the airplane CG,

$$C_{m_{cg}} = \frac{x_{cg}}{\bar{c}} C_{L_w} - \frac{l_h}{\bar{c}} \frac{S_h}{S_w} C_{L_h} + C_{m_w} + C_{m_{fus}} \quad (46)$$

and

Table 2: Variables in Eqn. 46

	$C_f$
$x_{cg}$	distance from wing aerodynamics center back to the CG
$\bar{c}$	mean aerodynamics chord
$C_{L_w}$	wing lift coefficient
$l_h$	distance from CG back to tail
$S_h$	horizontal tail reference area
$S_w$	wing reference area
$C_{L_h}$	tail lift coefficient
$C_{m_w}$	wing pitching moment coefficient (about the wing aerodynamics center)
$C_{m_{fus}}$	pitching moment of fuselage, nacelles, and other components (about CG)

To keep the airplane stable, the following requirement must meet,

$$\frac{\partial C_{m_{cg}}}{\partial C_L} < 0 \quad (47)$$

we approximate this derivative by differentiating the pitching moment coefficient equation with respect to the angle of attack,

$$\frac{\partial C_{m_{cg}}}{\partial \alpha} = \frac{x_{cg}}{\bar{c}} C_{L_{\alpha w}} - \frac{l_h S_h}{\bar{c} S_w} C_{L_{\alpha h}} + \frac{\partial C_{m_{fus}}}{\partial \alpha} \quad (48)$$

To find the natural point, we set the above equation to zero and solve it,

$$\frac{x_{np}}{\bar{c}} = \frac{l_h S_h}{\bar{c} S_w} \frac{C_{L_{\alpha h}}}{C_{L_{\alpha w}}} - \frac{1}{C_{L_{\alpha w}}} \frac{\partial C_{m_{fus}}}{\partial \alpha} \quad (49)$$

Therefore, the static margin can be calculated from,

$$S.M. = \frac{x_{np} - x_{cg}}{\bar{c}} = \frac{l_h S_h}{\bar{c} S_w} \frac{C_{L_{\alpha h}}}{C_{L_{\alpha w}}} - \frac{1}{C_{L_{\alpha w}}} \frac{\partial C_{m_{fus}}}{\partial \alpha} - \frac{x_{cg}}{\bar{c}} \quad (50)$$

The tail lift curve slope,  $C_{L_{\alpha h}}$  is affected by the pressure of the wing and the fuselage. In particular, the wing and fuselage produce downwash on the tail, and the fuselage boundary layer and contraction reduce the local velocity of flow over the tail; Thus,

$$C_{L_{\alpha h 0}} \left(1 - \frac{\partial \epsilon}{\partial \alpha}\right) \eta_h \quad (51)$$

where  $C_{L_\alpha}$  can be derived from the DATCOM formula,

$$C_{L_\alpha} \approx \frac{2\pi AR}{2 + \sqrt{(AR/\eta)^2(1 + \tan^2(\Lambda)) - M^2 + 4}} \quad (52)$$

where  $\eta = 0.97$ . More, for the advanced design purpose it is often possible to approximate the downwash at the tail by the downwash far behind and elliptically-loaded wing.

$$\epsilon \approx \frac{2C_{L_w}}{\pi AR_w}, \frac{\partial \epsilon}{\partial \alpha} \approx \frac{2C_{L_{aw}}}{\pi AR_w} \quad (53)$$

Gilruth developed and empirically-based method for estimating the effect of the fuselage,

$$\frac{\partial C_{m_{fus}}}{\partial C_L} = \frac{K_f w_f^2 L_f}{S_w \bar{c} C_{L_{aw}}} \quad (54)$$

where  $C_{L_{aw}}$  is the wing lift curve slope per radian,  $L_f$  is the fuselage length,  $w_f$  is the maximum width of the fuselage, and  $K_f$  is an empirical factor discussed in NACA TR711 and developed from an extensive test of wing-fuselage combinations in NACA TR50. We use the  $K_f = 0.487$  here.

## 6 OEW Model Validation

This section shows the weight validation process and results from existing vehicles by collecting and guessing the aircraft data to the weight model. The small multi-rotor vehicles have relatively large discrepancies ( $\approx 30\%$ ). We believe that the leading cause for these results is the fuselage length because the model is for the small aircraft, and as can be seen in Eqn. (2), aircraft weight is dominated by the maximum takeoff weight (MTOW). In contrast, we have relatively small errors (2% to 12%) for tilt-wing and tilt-rotor vehicles since their designed MTOW is in the range of small aircraft (2000 to 4000 lb).

### 6.1 Existing Multi-Rotor eVTOL

This section discussed the Operation Empty Weight (OEW) of varieties of multi-rotor eVTOL vehicles. Including EHang 184 [16] [3], EHang 216 [4][17][18]. We do not include the landing skid that both eVTOL have in the weight modeling process, and we got relatively large errors. Plus, the empty weight in Table. 3 is concluded to contain the battery weight since the sum of the empty and the battery weight (92 kg) equals the published maximum takeoff weight. Overall, we get relatively large errors in multi-rotor compared with the following eVTOL configurations. Moreover, the strut connecting the fuselage to the motor is not modeled either. It is hard to accurately model a multi-rotor vehicle since our model is mainly collected from aircraft and helicopters with very different geometries. More, the unique shape multi-rotor like Volocopter 2X 9b and 9a are also challenging to estimate the accurate weight since the existence of strut and fan duct.



(a) EHang 184



(b) EHang 216

Figure 8: Existing multi-rotor eVTOL, EHang 184 and EHang 216



(a) CityAirbus



(b) Volocopter 2X

Figure 9: Existing multi-rotor eVTOL, CityAirbus and Volocopter 2X

Table 3: Existing eVTOL vehicle specifications [3][4]

Specification	Units	EHang 184	EHang 216
Fuselage length	(m)	2.074	2.50(guessed)
Fuselage width	(m)	1.018	1.5(guessed)
Fuselage height	(m)	1.44	1.76
Nose landing gear	(m)	-	
Main Landing gear	(m)	-	
Propeller diameter	(m)	1.52	1.52
Number of propellers	-	8	
Number of motors	-	8	16
Number of passengers	-	1	2
Total motor rating	(kW)	152	
Cruise speed	(mph)	62	62
Maximum range	(mi)	9.9	22
OEW	(lb)	573.00	793.00
Battery weight	(kg)	92	-
Useful payload	(lb)	220.00	485.00
MTOW	(lb)	793.00	1322.00

Table 4: Comparison between published and modeled results for existing multi-rotor eVTOL

Component Weight	Units	EHang 184	EHang 216
Fuselage	(lb)	74.81	115.54
Equipment	(lb)	91.786	127.75
Total rotor and hub	(lb)	121.37	472.41
Total motor	(lb)	29.06	61.956
Total motor controller	(lb)	13.03	39.79
Designed Battery weight	(lb)	202.64	396.48(guessed)
Payload	(lb)	220.00	485.00
Published OEW	(lb)	572.68	808.46
Estimated OEW (with battery)	(lb)	778.26	1189.48

## 6.2 Existing Tilt-Wing eVTOL

We use Airbus A<sup>3</sup>Vahana  $\beta$  for tilt-wing eVTOL weight validation in this section. The data from the vehicle are collected from verities resources [19][5]. Data that cannot be found in the online resources nor literature above are measured and guessed from the 10. It is worth noticing that the aircraft height listed in Fig. 10 is 9.75 feet, which does include the landing skids of the aircraft. To address this problem, we do not include the landing gear data into the Airbus A<sup>3</sup>Vahana  $\beta$  model. We assume that the over-estimated fuselage height compensates for the landing gear weight. As a result, the weight validation result is shown in Table. 6 represent small errors in operation empty weight. We need more aircraft data like this to

decide whether we can use the total aircraft height instead of fuselage height for eVTOL size as well as configuration like Airbus  $A^3$ Vahana  $\beta$ .

Table 5: Existing tilt-wing eVTOL vehicle specifications [5]

Specification	Units	Airbus $A^3$ Vahana $\beta$
Fuselage length	(ft)	19.5
Fuselage width	(ft)	(estimated) 5.00
Fuselage height	(ft)	9.275
Wingspan	(ft)	20.6
Wing Area	(ft <sup>2</sup> )	96.88
Horizontal stabilizer area	(ft <sup>2</sup> )	
Vertical stabilizer area	(ft <sup>2</sup> )	(estimated) 24.31
Nose landing gear	(ft)	-
Main Landing gear	(ft)	-
Propeller diameter	(ft)	(estimated) 5.07
Number of propeller(s)	-	8
Number of motor(s)	-	8
Number of passenger(s)	-	2
Total motor rating	(kW)	360
Cruise speed	(mph)	142.92
Maximum range, without reverse	(mi)	60
OEW	(lb)	1050
Battery weight	(kg)	202.64
Useful payload	(lb)	450
MTOW	(lb)	1800

Table 6: Existing tilt-wing vehicle calculated OEW

Modeled Weight	Units	Airbus $A^3$ Vahana $\beta$
Structure	(lb)	260.60
Equipment	(lb)	146.78
Total rotor and hub	(lb)	247.66
Total motor	(lb)	273.76
Total motor controller	(lb)	145.15
Modeled OEW	(lb)	1073.95
Published OEW	(lb)	1050.00

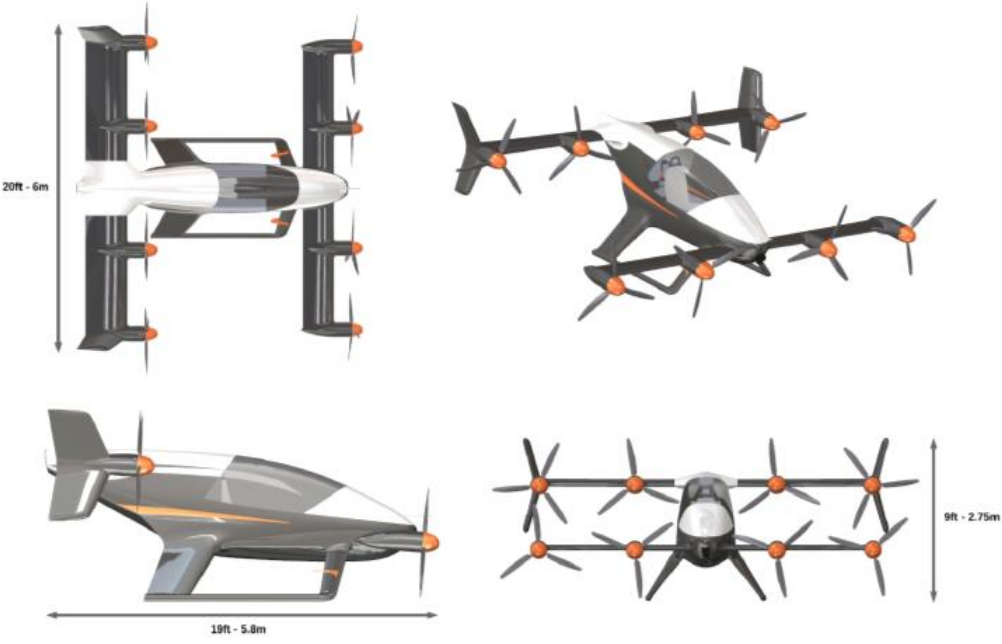


Figure 10: Dimension of Airbus A<sup>3</sup>Vahana

### 6.3 Existing Tilt-Rotor eVTOL

We used Archer maker, Joby S4, as well as Duffy's literature for tilt-rotor validation. Most of the aircraft specifications are collected from either office website or published data from [7] [6]. Again, we use the unpublished specifications by considering a similar aircraft, literature paper, and existing counterparts to estimate each component's series of reasonable values. For example, the fuselage length and height guessed from a conventional mid-size family car as well as helicopter. We assumed that the weight these companies published on their website is the empty weight without batteries.



(a) Joby S4

(b) Archer two seater maker

Table 7: Existing tilt-rotor vehicle specifications [6][7]

Specification	Units	Archer Maker (2-seater)	Joby S4
Fuselage length	(ft)	42	25
Fuselage width	(ft)	5 (estimated)	5.8 (estimated)
Fuselage height	(ft)	6 (estimated)	5.8 (estimated)
Wingspan	(ft)	40	40 (estimated)
Wing Area	(ft <sup>2</sup> )	129.17	122.49
Horizontal stabilizer area	(ft <sup>2</sup> )	-	-
Vertical stabilizer area	(ft <sup>2</sup> )	34.44 (V-tail, estimated)	40 (V-tail, estimated)
Nose landing gear	(ft)	2(estimated)	2(estimated)
Main Landing gear	(ft)	3.2(estimated)	3(estimated)
Propeller diameter	(ft)	3.94(estimated)	9.5
Number of propellers	-	6	
Number of motors	-	6	
Number of passengers	-	2	4 + 1(crew)
Total motor rating	(kW)	325	480
Cruise speed	(mph)	150	200
Maximum range, without reverse	(mi)	60	200
OEW	(lb)	3324.57	-
Useful payload	(lb)	480 (estimated)	960(estimated)
Battery weight	(lb)	-	-
MTOW	(lb)	4000 (estimated)	4000 (estimated)

Table 8: Comparison between published and modeled results for existing tilt-rotor eVTOL

Modeled Weight	Units	Archer Maker	Joby S4	Duffy's tilt-rotor
Structure	(lb)	1233.95	1052.69	670.129
Equipment	(lb)	225.46	37.33	283.23
Total motor	(lb)	954.46	222.31	871.87
Total motor controller	(lb)	137.31	511.34	470.08
Total rotor and hub	(lb)	1081.28	182.06	416.30
Modeled OEW	(lb)	3107.27	2782.63	2711.61
Published OEW	(lb)	3324.57	3160	2596.00

## 7 Reproduce Literature Flight Mission

From Kadhiresan [8], the mission segment is provided in the following Table for tilt-rotor eVTOL sizing validation. The mission contains vertical takeoff, cruise, and vertical landing that can be summarized in Table, 9. The reason to use this model for our weight validation is that we use some of the components in the empty operation weight model in section 5.1—the eVTOL data from Table. 10 is used for the mission segment mentioned in Table. 9. Figure 12a from Table shows a mission profile for given inputs. We then validate the optimal

model from the result Kadhiresan [8] provided, the vehicle specifications have also been provided in the same literature. The optimal model from the published data is obtained by minimizing the maximum takeoff weight (MTOW). The analysis results are shown in Fig. 13.

Table 9: Mission profile validation for tilt-rotor vehicle

Stage	Mission Segment	Mission Specification	Duration (min)
1	Takeoff	Rate of Climb: 750 fpm	2
2	Cruise	Cruise speed: 100 mph	17.14
3	Landing	Rate of Climb: -750 fpm	2

Figure. 13f give a series of analysis results from the model we have developed so far. All x-axes represent the integral time results integrated from the OpenConcep solver. It is worth noticing that in Fig. 13b the throttle increase gradually with respect to the flight altitude, which is reasonable since the air density is lower in a higher altitude. One assumption that may be assumed is that the propeller efficiency is not high enough during the takeoff phase; thus, the change in the thrust is prominent. Following this idea, we can see that it is reasonable to have a faster energy consumption in the vertical takeoff phase than the cruise phase in Fig. 13d.

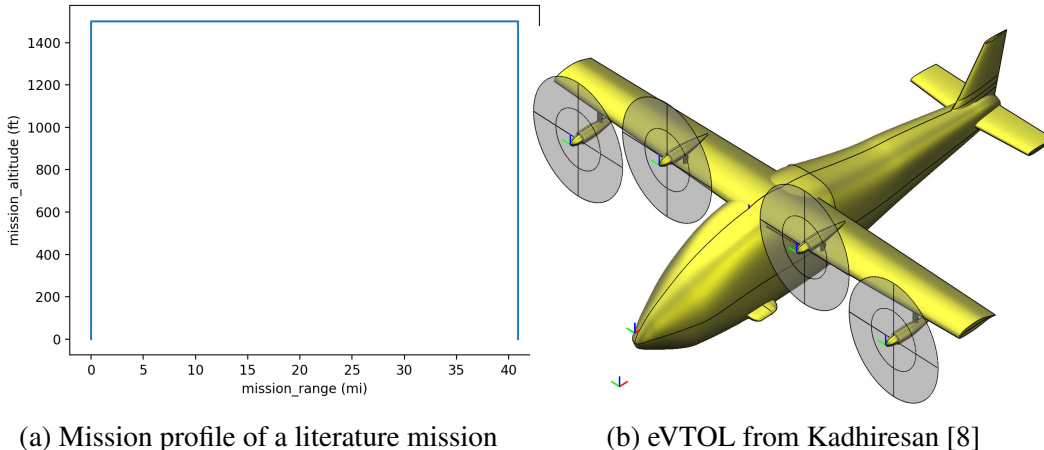


Figure 12: Figures for the mission validation

For the weight model in this section, a small error ( $\approx 10\%$ ) is shown in Table. 10. However, since not much data from the resource, we again estimated the eVTOL data from experience in Table. 7 and also the figure in the literature. The landing gear size is also guessed based on a small aircraft like Cessna or Beechcraft Bonanza since Figure 12b is in a similar geometries as well as fuselage shape to existing small aircraft to them. Also, the empennage areas are guessed in the same fashion.

Table 10: Comparison and sizing validation for a tilt-rotor eVTOL

Parameters	Units	Estimated	Published [8]
Wing Area	ft <sup>2</sup>	257.2	161.5
Wing Span	ft	50.0	33.61
AR	-	9.72	7.0
Fuselage length	ft	50	50
Fuselage width	ft	5.8	5.8
Fuselage height	ft	5.8	5.8
Vertical stabilizer area	ft <sup>2</sup>	25	25
Horizontal stabilizer area	ft <sup>2</sup>	40	40
Nose landing gear	ft	3	3
Main landing gear	ft	4	4
Number of propellers	-	2	2
Propeller Diameter	ft	20	20
Single Motor power	kW	-	282 kW
Empty weight	lb	2596	2277.30
Battery Weight	lb	462	882.44
Payload	lb	800	800.00
MTOW	lb	3858	3959.74

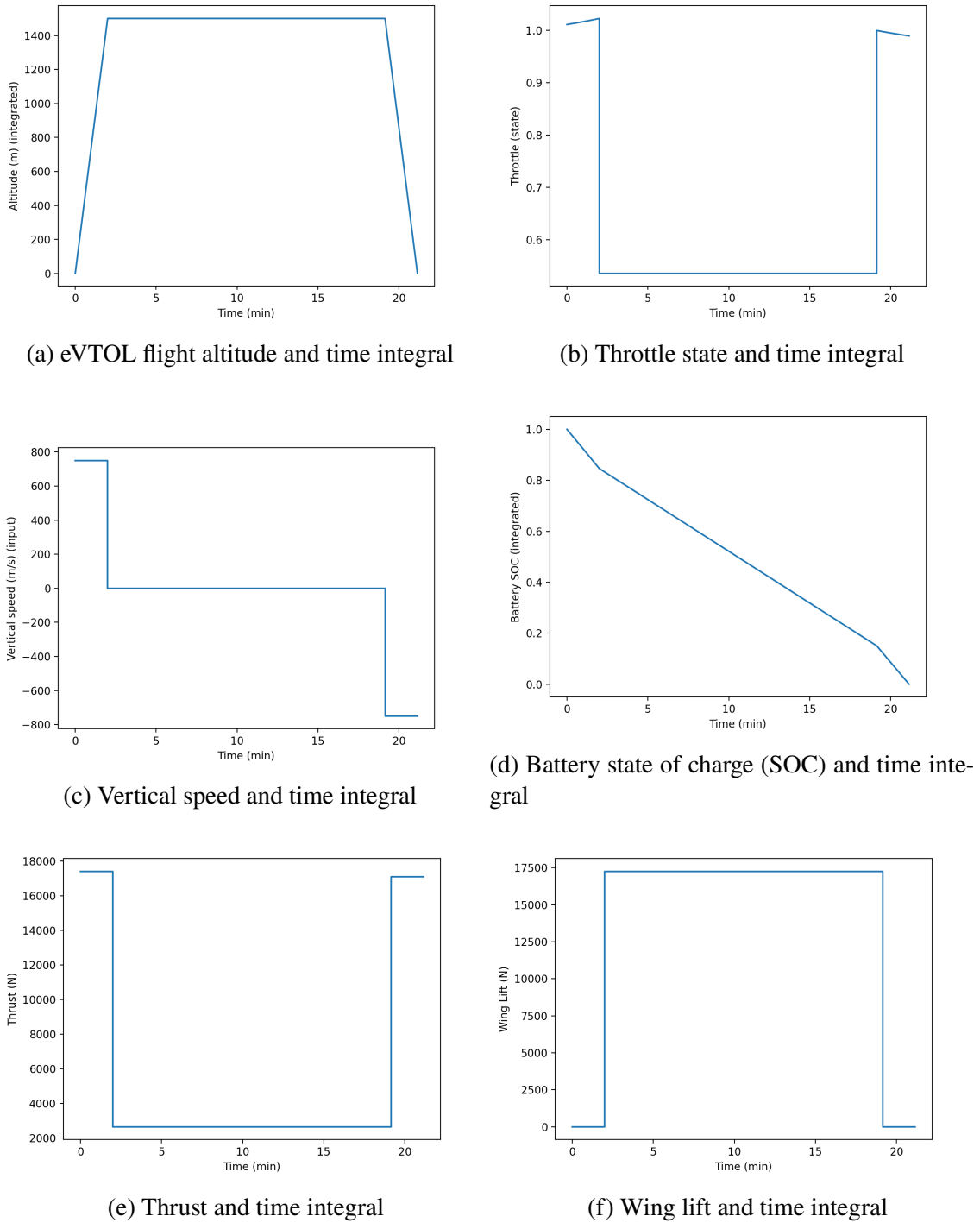


Figure 13: Mission analysis validation result plots

## 8 Multidisciplinary Design Optimization Study

This section provides a series of studies that the reader may be interested in. The first subsection is the optimization from the Kraenzler [10] by using the SLSQP [20] optimizer in

the last semester. In this semester, the studies of minimum MTOW, and extreme range across eVTOL configurations study performed by SNOPT [21] are added to this report providing readers more insight into eVTOL conceptual design. The optimizer benchmarking is provided in the appendix.

## 8.1 Optimizing Literature case for On-demand Mission Requirement

### 8.1.1 Problem Formulation

The mission segment for the multidisciplinary design optimization is modified from the Kraenzler [10]. The goal in this section is to minimize the tilt-rotor case from Kraenzler [10] for the UberAir requirement[22] requirement accompany by the aircraft data in Table 10. The range is measured from the vertical takeoff to the vertical landing phases. The vehicle first vertical takeoff to 500 ft, which is the minimum safe altitude for general aircraft in the congested areas, then climbs to 1500 ft above the highest building. We used the cruise altitude of 1500 ft to simulate the general condition [23] and UberAir requirement[22]. The visualization of the mission profile is shown in Fig. 14.

Table 11: Mission profile optimization validation

Stage	Mission Segment	Mission Specification	Duration (min)
1	Vertical takeoff	Rate of Climb: 500 fpm	3
2	Cruise	Cruise speed: 150 mph	24
3	Vertical landing	Rate of descend: 500 fpm	3

In this section, only the tilt-rotor configuration is considered in this report. This report used and assumed the published data from Jody S4[7] and Archer Maker[6] to simulate a two-to-four-seated tilt-rotor eVTOL for the mission given in the Table [11]. After the optimization validation section, the data shown in Table 13 was used as aircraft data in the following Multidisciplinary Design Optimization (MDO) study.

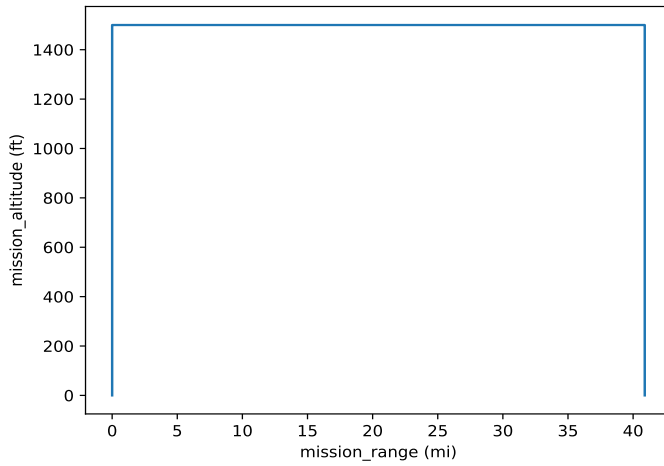


Figure 14: Mission profile of MDO validation

We use the similar approaches mentioned in Table 10 that guess some of the eVTOL geometries from the vehicle's shape and published images. The multidisciplinary design optimization process is formulated in Table 12

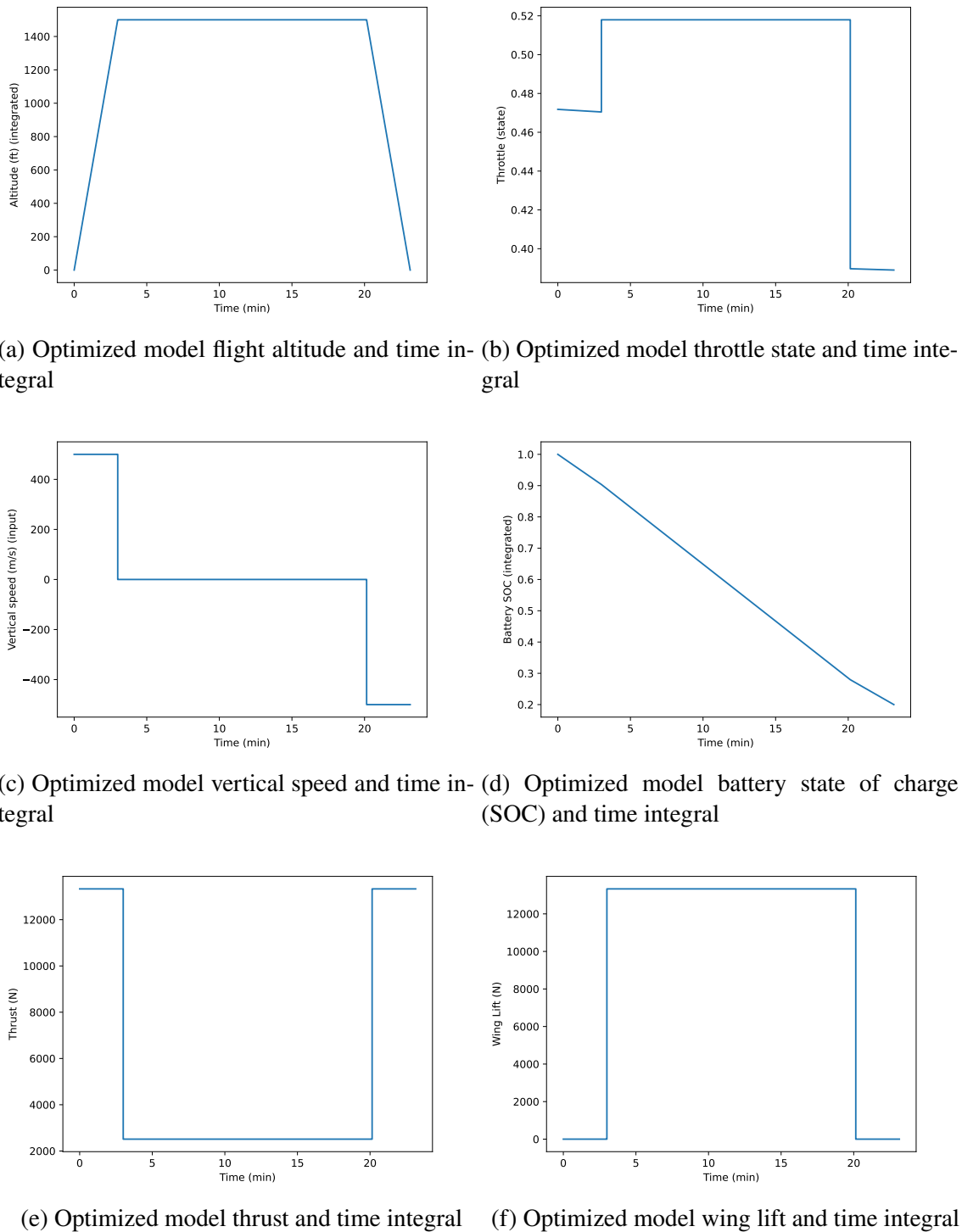


Figure 15: Mission analysis validation result plots

Table 12: Tilt-rotor setup for on-demand validation

	Function/ Variable	Description	Bounds
minimize	MTOW	Maximum takeoff weight, lb	
given	$\rho_{\text{battery}}$	battery energy density, Wh/kg	
	$V_{\text{cruise}}$	Cruise velocity, mph	
	Payload	Payload, kg	
wrt	MTOW	MTOW, lb	[100, ]
	$S_{\text{wing,ref}}$	Wing reference area, ft <sup>2</sup>	[170, ]
	AR	Wing aspect ratio	[8, ]
	$S_{\text{vstab,ref}}$	Vertical stabilizer reference area, ft <sup>2</sup>	[50, ]
	$L_{\text{fuselage}}$	Fuselage length, ft [50, ]	
	$\phi$	One Propeller diameter, ft	[15, ]
	$W_{\text{battery}}$	Total battery weight, lb	[10, ]
	$P_{\text{single}}$	One Motor rating. kW	[200, ]
subject to	$\text{MTOW} - W_{\text{payload}}$	Making MTOW residual to zero	
	$- W_{\text{battery}} - \text{OWE} = 0$		
	Final SOC <sub>battery</sub> = 0.2	Final battery SOC [24]	
	$\eta_{\text{propeller, takeoff}} \geq 0.8$	Propeller efficiency during takeoff	
	$\text{RPM} \leq \text{RPM}_{\text{max}}$	Maximum RPM	
	$1 \geq \text{takeoff throttle} \geq 0$	Takeoff throttle	
	$1 \geq \text{landing throttle} \geq 0$	Landing throttle	

Table 13: On-demand mission requirement optimization result

Parameters	Units	Published [8]	Optimized model
Wing Area	ft <sup>2</sup>	257.2	170
Wing Span	ft	50.0	50
AR	-	9.72	8.0
Fuselage length	ft	50	50
Fuselage width	ft	5.8	5.8
Fuselage height	ft	5.8	5.8
Vertical stabilizer area	ft <sup>2</sup>	25	25
Horizontal stabilizer area	ft <sup>2</sup>	25	40
Nose landing gear	ft	3	3
Main landing gear	ft	4	4
Number of propellers	-	2	2
Propeller Diameter	ft	20	20
Single Motor power	kW	320	200
Empty weight	lb	2596	1499.89
Battery Weight	lb	462	697.096
Payload	lb	800	800.00
MTOW	lb	3959.74	2996.98

### 8.1.2 Results and Discussion

Table 13 that the optimized model has a 1000 lb discrepancy in weight compared with the published model. This can be attributed to a lower wing area, an aspect ratio of an optimized model. Since the optimizer found the minimum MTOW, it would find the minimum feasible wing dimension that could generate enough lift force for the cruise segment. The optimizer also finds a lower motor rating required for the same mission profile. Figure. 15 gives some flight parameters regarding the mission. In the Fig. 15b, the throttle in the landing was significantly different from the last semester's work in Fig. 13b since we implement the momentum theory in the vertical takeoff and landing segment and also considered the vortex ring state during the landing segment.

## 8.2 MTOW minimization

### 8.2.1 Problem Formulation

Among many aircraft conceptual design topics, the Maximum Takeoff Weight (MTOW) is always the most interesting topic for the aircraft designer. By knowing the MTOW, the aircraft designers can have a brief overview of the trend of each component or power consumption and, therefore, estimate the cost of a particular aircraft type. In sum, the estimation of MTOW plays a critical role in aircraft conceptual design. In this report, an MTOW of three types of configuration of eVTOL, EHang 216 3, CityAirbus3, and JobyS4 8 was investigated, the detailed optimization setup was provided below, for empennage and wing were suppressed for the multi-rotor cases that do not equip such component.

Table 14: MTOW minimization problem for EHang 216-class vehicle

	Function/ Variable	Description	Bounds
minimize	MTOW	Maximum takeoff weight, lb	
given	$\rho_{\text{battery}}$	battery energy density, Wh/kg	
	$V_{\text{cruise}}$	Cruise velocity, mph	
	Payload	Payload, kg	
wrt	MTOW	MTOW, lb	[100, ]
	$L_{\text{fuselage}}$	Fuselage length, m	[2.5, ]
	$\phi$	One Propeller diameter, ft	[5, ]
	$W_{\text{RPM}}$	Rotor RPM, rpm	[300, ]
	$W_{\text{battery}}$	Total battery weight, lb	[10, ]
	$P_{\text{single}}$	One Motor rating. kW	[10, ]
subject to	$\text{MTOW} - W_{\text{payload}} - W_{\text{battery}} - \text{OEW} = 0$	Making MTOW residual to zero	
	$\text{Final SOC}_{\text{battery}} = 0.2$	Final battery SOC [24]	
	$\text{RPM} \leq \text{RPM}_{\max}$	Maximum RPM	
	$1 \geq \text{takeoff throttle} \geq 0$	Takeoff throttle	
	$1 \geq \text{cruise throttle} \geq 0$	Cruise throttle	
	$1 \geq \text{landing throttle} \geq 0$	Landing throttle	

Table 15: MTOW minimization problem for CityAirbus-class vehicle

	Function/ Variable	Description	Bounds
minimize	MTOW	Maximum takeoff weight, lb	
given	$\rho_{\text{battery}}$	battery energy density, Wh/kg	
	$V_{\text{cruise}}$	Cruise velocity, mph	
	Payload	Payload, kg	
wrt	MTOW	MTOW, lb	[100, ]
	$L_{\text{fuselage}}$	Fuselage length, m	[8, ]
	$\phi$	One Propeller diameter, ft	[9.2, ]
	$W_{\text{RPM}}$	Rotor RPM, rpm	[300, ]
	$W_{\text{battery}}$	Total battery weight, lb	[10, ]
	$P_{\text{single}}$	One Motor rating. kW	[10, ]
subject to	$\text{MTOW} - W_{\text{payload}} - W_{\text{battery}} - \text{OWE} = 0$	Making MTOW residual to zero	
	$\text{Final SOC}_{\text{battery}} = 0.2$	Final battery SOC [24]	
	$\text{RPM} \leq \text{RPM}_{\max}$	Maximum RPM	
	$1 \geq \text{takeoff throttle} \geq 0$	Takeoff throttle	
	$1 \geq \text{cruise throttle} \geq 0$	Cruise throttle	
	$1 \geq \text{landing throttle} \geq 0$	Landing throttle	

Table 16: MTOW minimization problem for JobyS4-class vehicle

	Function/ Variable	Description	Bounds
minimize	MTOW	Maximum takeoff weight, lb	
given	$\rho_{\text{battery}}$	battery energy density, Wh/kg	
	$V_{\text{cruise}}$	Cruise velocity, mph	
	Payload	Payload, kg	
wrt	$S_{\text{wing,ref}}$	Wing reference area, $\text{m}^2$	[16, ]
	AR	Wing aspect ratio	[7, ]
	$S_{\text{vstab,ref}}$	Vertical stabilizer reference area, $\text{ft}^2$	[35, ]
	$L_{\text{fuselage}}$	Fuselage length, ft [20, ]	
	$\phi$	One Propeller diameter, ft	[9.5, ]
	$W_{\text{battery}}$	Total battery weight, lb	[10, ]
	$P_{\text{single}}$	One Motor rating. kW	[10, ]
subject to	$\text{MTOW} - W_{\text{payload}} - W_{\text{battery}} - \text{OWE} = 0$	Making MTOW residual to zero	
	$\text{Final SOC}_{\text{battery}} = 0.2$	Final battery SOC [24]	
	$\eta_{\text{propeller, takeoff}} \geq 0.8$	Propeller efficiency during takeoff	
	$\text{RPM} \leq \text{RPM}_{\max}$	Maximum RPM	
	$1 \geq \text{takeoff throttle} \geq 0$	Takeoff throttle	
	$1 \geq \text{landing throttle} \geq 0$	Landing throttle	

### 8.2.2 Results and Discussion

Figure 16 gave results of minimizing the MTOW by sweeping the payload and cruise speed with respect to three different types of eVTOL.

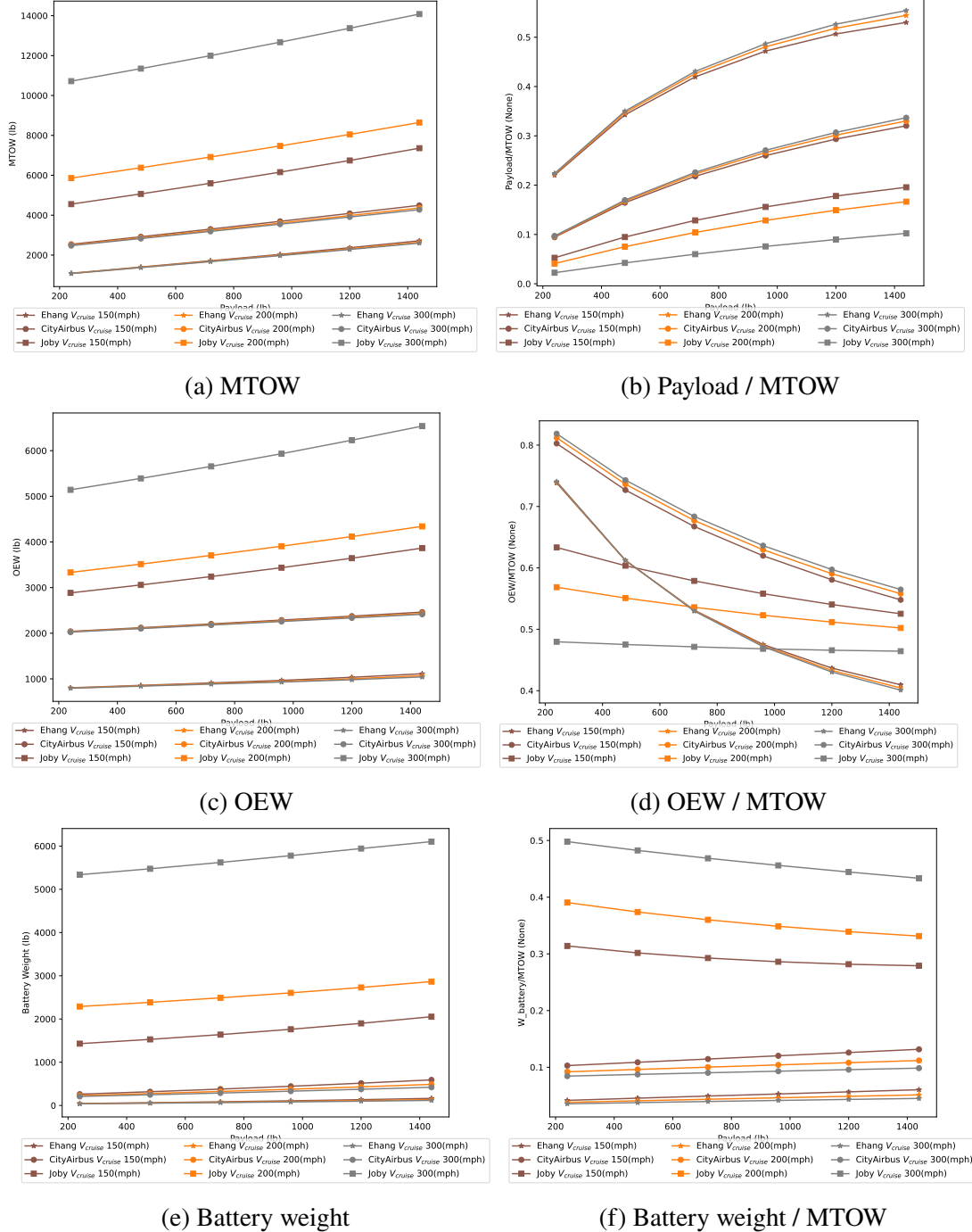


Figure 16: Aircraft weights ratio of MTOW minimization

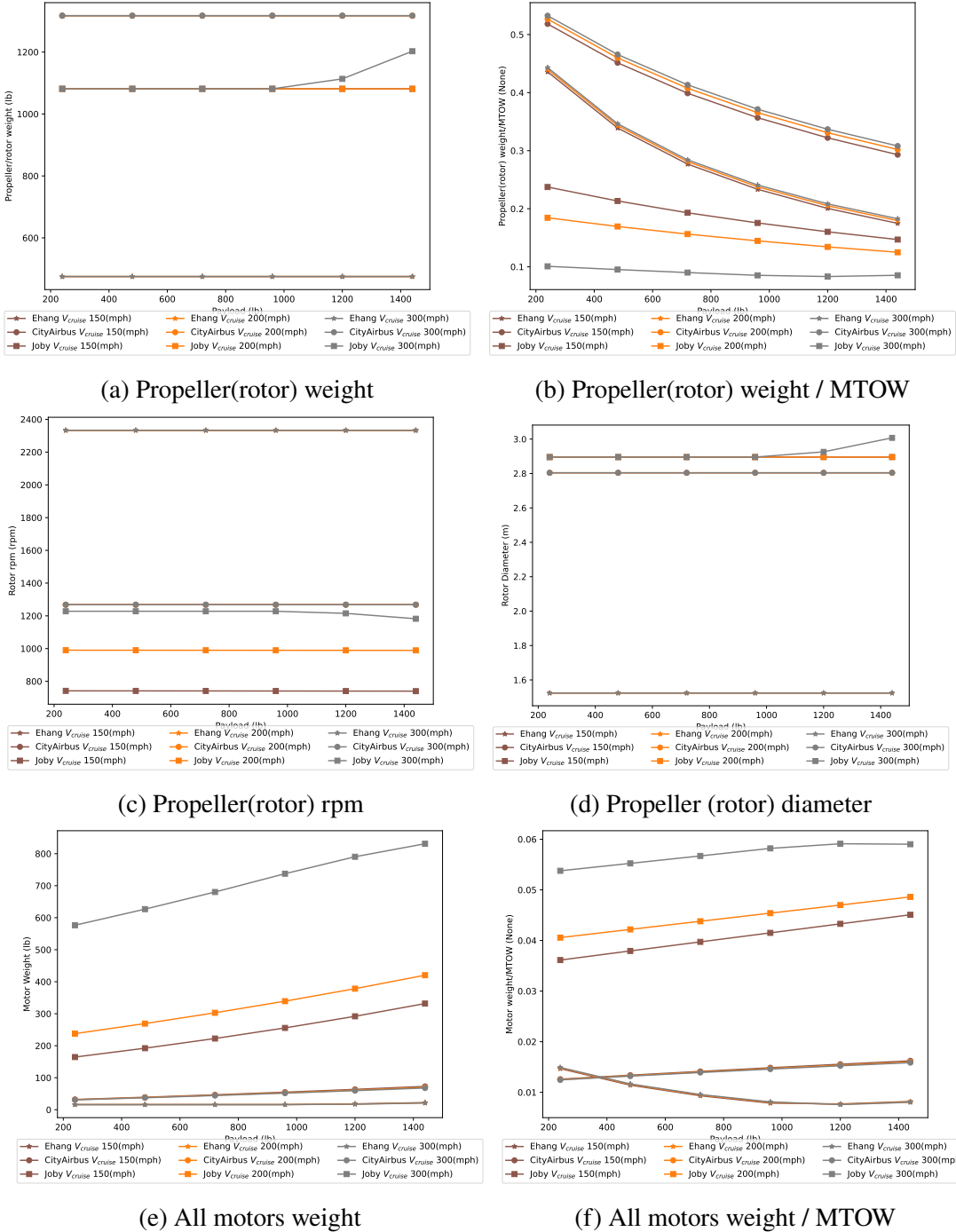


Figure 17: Component weights ratio of MTOW minimization

Figure 16a shows an intuitive trend on changing MTOW. The EHang216 and CityAirbus have lower overall MTOW in terms of different payloads. Also, the MTOW change is not significant for EHang216 and CityAirbus from a cruise speed of 150 [mph] to 300 [mph]. On the other hand, the JobyS4 model changes in different cruise speeds. The MTOW doubles when the cruise speed doubles, which cannot be seen on the multi-rotor configuration. We can look at the propulsion component weight from Fig. 16b, the increase rate of payload-to-

MTOW ratio decreased as payload increased. And the trend has a small change for different cruise speeds in multi-rotor configuration and a large ratio change for the tilt-rotor model. The OEW values in fig. 16c, the OEW had good fit to the MTOW trend shown in the Fig. 16a. However, Fig. 16d negate this guess since the OEW-to-MTOW ratio decreasing as payload increasing. Figure 16e gave a view of increasing battery weight but again decreasing Battery-Weight-to-MTOW-ratio. Figure 17c and Figure 17d shows that the optimizer consistently hits the lower bound of the propeller(rotor) diameter and RPM when finding the minimum MTOW for almost every model in every payloads and cruise speed. One possible explanation can be the optimizer found the minimum thrust produced possible for each run to minimize the OEW since this report uses the basic momentum theory, assumes the steady flight, and ignores the aeroacoustics and detailed rotor design parameters. Lacking these detailed considerations can cause hitting the lower bound of the propeller(rotor) RPM and diameter. Also, in Fig. 17b, the tilt-rotor has an overall lower propeller(rotor)-to-weight ratio compares with the other two configurations since the tilt-rotor eVTOL also has wings and over control surface. On the other hand, multi-rotor tend to have a higher propeller(rotor)-weight-to-MTOW ratio since most weights are contributed by the propulsion system rather than wings and control surfaces. The last thing that contributed to increasing MTOW was the motor weight, as shown in Fig. 17e and Motor-to-MTOW ratio in Fig 17f. Figure 17f give a clear view that the Motor-to-MTOW ratio increased as payload increased for the CityAirbus and JobyS4 but EHang216. The one possible reason that EHang216 had a different motor weight trend is that it has 16 rotors, and there is no need to produce that much power for each motor and thus has a shallower slope compared to the other two configurations.

To further investigate the reason why tilt-rotor has such a huge difference from the other two configurations, Fig18 might give some insights. The aerodynamics model implemented for a tilt-rotor is different from the multi-rotor configuration. In the tilt-rotor model, we use the polar drag to estimate the aerodynamics drag when cruising. More, the air density affected the aerodynamics drag. Since our target cruise altitude is 1500 ft, far less than the usual winged aircraft, a higher air density leads to a higher aerodynamics drag at the lower cruising altitude. However, the drag model used in the multi-rotor is described in Eqn.40, which is a constant ratio between the rotor angle of attack and thrust generated by a single rotor, therefore has little effect on the cruise speed.

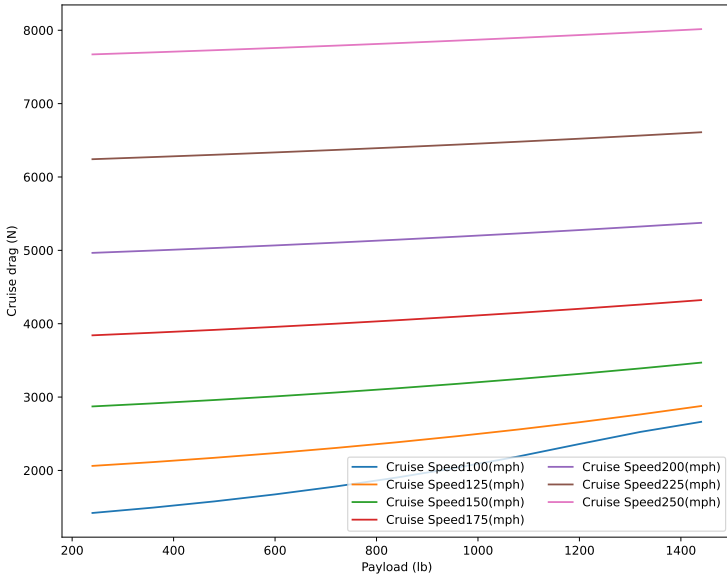


Figure 18: Tilt-rotor cruise drag

### 8.3 Extreme Range Study Across eVTOL Configurations

One another interesting topic for the eVTOL conceptual study is the extreme study. By doing this study, we can predict the weight and energy trend of different eVTOL configurations. Therefore, this report focuses on investigating the maximum range for on-demand eVTOL. Further, three types of eVTOL, EHang216, CityAirbus, and JobyS4, are performed in this study. Further, the detailed setup for each eVTOL can be found in the previous Table 14, Table 15, and 16 for each eVTOL. The only different setup from the section 8.2 is that we are exploring the maximum range in this section.

#### 8.3.1 Problem Formulation

To match the real-world scenario, the vehicle was targeted to have a cruise speed of 150 mph, a cruising range of 60 miles, with 980 [lb] of usable payload defined by Uber Elevate [22].

#### 8.3.2 Results and Discussion

From Fig. 19a, the sign of increasing MTOW appears for all three models, as expected. For the tilt-rotor eVTOL, MTOW doubles when the cruise range changes from 60 miles to 120 miles, but both multi-rotor cases show a relative MTOW increment across the range. Also, a tilt-rotor has a short useful range compared with the multi-rotor model, which is not intuitive. Moreover, a reasonable explanation is that in this report, the aircraft dimension wasn't changed to payload accordingly. That means, for example, a 2-seater EHang216 had the same 2.5-meter-long fuselage even though it has four passengers and a larger battery. Moreover, this can lead to a problem since many component weight estimation models de-

pend on all aircraft dimensions and MTOW. In Fig. 19b, for a tilt-rotor, a payload-to-MTOW ratio drops nearly 50% when the cruise range increases from 60 miles to 240 miles, which not only be seen in the EHang216 model but also CityAirbus. On the other hand, due to other aircraft component weight, the payload-to-MTOW ratio dropped drastically from 20% to 8% in from cruise range of 60 miles to 210 miles. That being said, the payload ratio drops 50% when the distance doubles. Figure 19c and Figure 19d show a trend of how OEW change with the usable range. Again, the OEW increases with the cruise range, just like MTOW expected. Only EHang216 increase the OEW-to-MTOW ratio for longer ranges, but the OEW-to-MTOW ratio stays near the 65% to 45% from the 60 to 240 miles for all three cases. And 19f shows the 5% to 30% of overall battery-weight-to-MTOW ratio to CityAirbus and EHang216 model; and 20% to 47% of battery ratio for the JobyS4 tilt-rotor model. Again, like in the section8.2, the propeller(rotor) diameter 20d and rpm 20c hits the lower bound during the optimization. Also, the motor weight has a fit trend to the OEW changes but is not as significant to the battery weight ratio.

The results seem to be non-intuitive. The optimizer constantly hits the lower bound of design variables. These issues may be caused by lacking proper constraints, improper assumptions, and critical models.

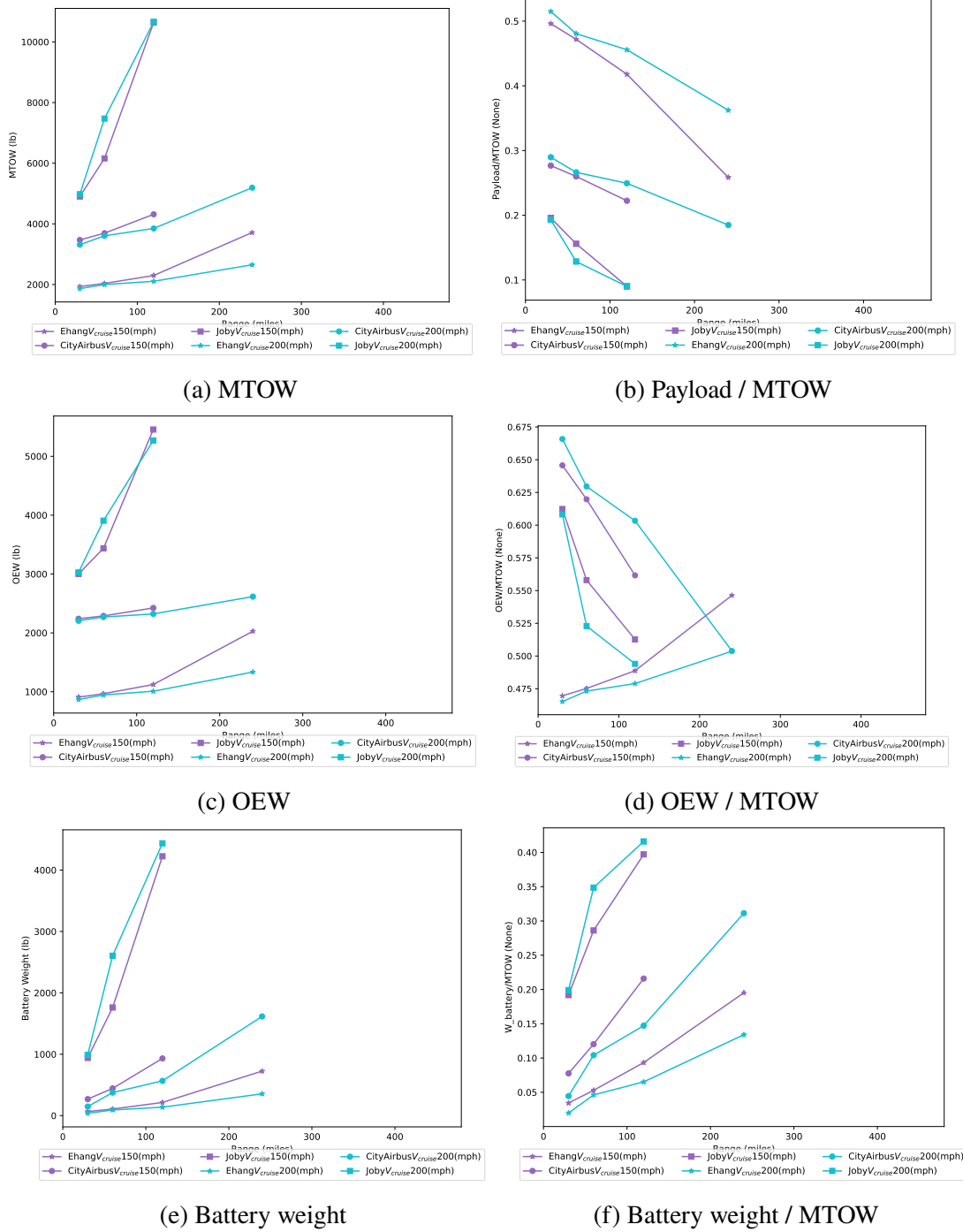


Figure 19: Aircraft weights and MTOW ratio results of extreme range studies

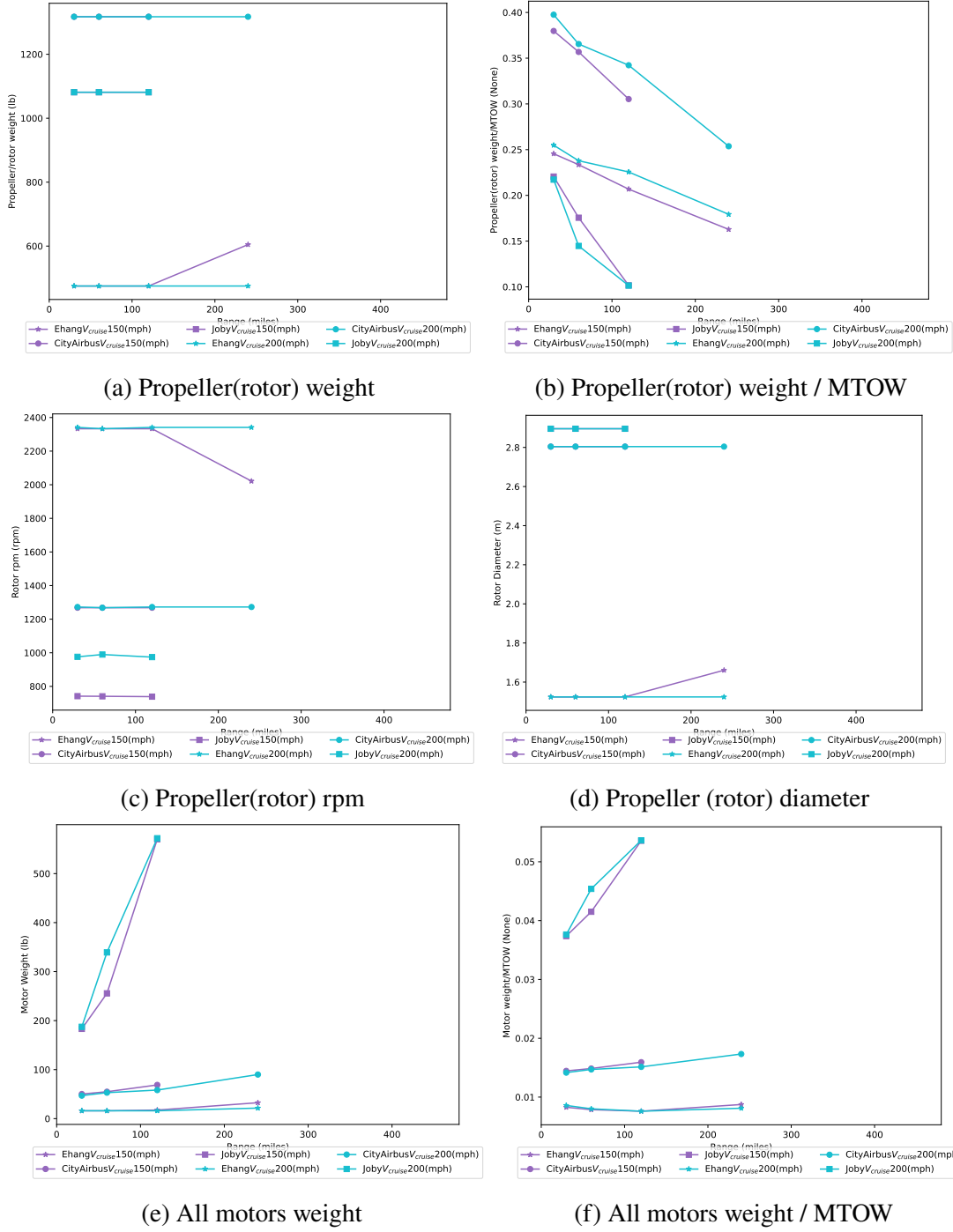


Figure 20: Aircraft Component weights and MTOW ratio results of extreme range studies

## 9 Summary

This eVTOL conceptual tool kit is inspired by the existing example in the OpenConcpet, an open-source MDAO software based on NASA's OpenMDAO framework. We first investigate, create, and validate a weight estimation model. In this model, various aircraft such

as conventional small fixed-wing aircraft and helicopter models are considered. Our weight model shows relatively larger multi-rotor model errors in the validation section, which can be concluded with the unique shape and additional structure from existing multi-rotor configurations. In contrast, the heavier model has good accuracy ( $\approx 12\%$ ).

The multidisciplinary design optimization studies are conducted to minimize the maximum takeoff weight (MTOW). The minimizing MTOW results show that the motor weights are highly similar to the MTOW weight trends; The battery weight changes have a higher sensitivity to a cruise speed than the payload for an eVTOL. The MDO validation gives a brief overview that the optimized model we have developed seems to have a high tendency hit the lower bound of wing area, aspect ratio, and motor rating to keep a minimum condition to complete the mission; And, therefore, have a discrepancy in MTOW compared with the published model. The minimum MTOW study again shows a sign of encountering a lower bound in propulsion wing aspect ratio, propeller diameter, and motor rating. The difference in propulsion models through this report makes counter-intuitive results that the tilt-rotor has a larger maximum MTOW than the other two tilt-rotor models with the same payload and cruise speed. EHang216 equips 16x of 5 feet-propeller, which can generate a great amount of trust in our model. However, as mentioned before, we assumed EHang could carry 6 passengers in a 2-seater eVTOL, which can be improved in a future study. The extreme study shows a sign of the 45% to 65% of OEW-to-MTOW ratio across the maximum range and the battery-to-MTOW ratio of 5% to 30% for three kinds of eVTOL, which could be useful for the future eVTOL designer. The final topic in the MDO study is optimizer benchmarking, which indicates that SNOPT has a better performance in terms of function calls.

## 10 Future Work

**Classification of eVTOL** Some directions can be investigated and improved in the future. The first way is to classify the aircraft according to the payload. The same type of eVTOL must have two kinds of dimensions for different payload ranges. For example, for a tilt-rotor model, we can have a size of Cessna-Turbo Stationair HD first for passengers under 6 and have a size like Cessna Caravan for 6 to 14 passengers. The second approach is to classify aircraft like [8] to define a specific box for different eVTOL types.

**Aerodynamics and energy consumption model** Improvements in aerodynamics and propulsion models can be investigated in the future, such as the multi-rotor configuration's drag coefficient. This improvement could be made by investigating more literature to find the best fit for our model. More, as discussed in the MDO study, some works can be investigated: to relieve the lower bound of the propeller diameter, modify the existing power consumption model, and create a more critical propulsion model for multi-rotor configuration.

**Stability Analysis** Also, including the stability analysis can improve the current model. For the current model, the optimizer always hits the lower bound of the control surfaces. Introducing flight dynamics parameters such as the center of gravity and static margin can increase the importance of control surfaces.

**Cost Analysis** As for new topics that can be interesting, the cost model is beneficial for a business entity for capturing the cost of energy consumption and maintenance. Also, the charging time estimation can be useful and, therefore, added to the MDO study to find the optimum ways to operate an eVTOL fleet. Last, since some existing eVTOL companies use the hybrid configuration that an eVTOL equips the lift and course propeller, this feature could make our model more realistic. Also, the motor failure condition can be investigated to comply with the FAA regulation.

## References

- [1] mccauley, “Constant speed propeller search result.” <https://mccauley.txtav.com/>, 2021. [Online; accessed 30-November-2021].
- [2] D. B. Play., “Design fridays: That’s a big prop.” <https://frautech.wordpress.com/2011/01/28/design-fridays-thats-a-big-prop/>, JANUARY 28, 2011. [Online; accessed 8-December-2021].
- [3] E. V. F. Society, “EHang 184 (defunct).” <https://evtol.news/ehang/>, 2017. [Online; accessed 7-December-2021].
- [4] E. V. F. Society, “EHang 216.” <https://evtol.news/ehang-216/>, 2017. [Online; accessed 7-December-2021].
- [5] E. V. F. Society, “A<sup>3</sup> vahana (defunct).” <https://evtol.news/a3-by-airbus/>, 2019. [Online; accessed 8-December-2021].
- [6] NASA, “Analysis and full scale testing of the joby s4 propulsion system.” <https://nari.arc.nasa.gov/sites/default/files/attachments/Stoll-TVFW-Aug2015.pdf>, 2015. [Online; accessed 7-December-2021].
- [7] Archer, “Archer maker.” <https://www.archer.com/maker>, 2021. [Online; accessed 8-December-2021].
- [8] A. R. Kadhiresan and M. J. Duffy, “Conceptual design and mission analysis for evtol urban air mobility flight vehicle configurations,” in *AIAA Aviation 2019 Forum*, p. 2873, 2019.
- [9] B. J. Brelje and J. R. R. A. Martins, “Development of a conceptual design model for aircraft electric propulsion with efficient gradients,” in *2018 AIAA/IEEE Electric Aircraft Technologies Symposium*, no. AIAA-2018-4979, (Cincinnati, OH), July 2018.
- [10] M. Kraenzler, M. Schmitt, and E. Stumpf, “Conceptual design study on electrical vertical take off and landing aircraft for urban air mobility applications,” in *AIAA Aviation 2019 Forum*, p. 3124, 2019.
- [11] R. Prouty, *Helicopter Performance, Stability, and Control*. R.E. Krieger Publishing Company, 1995.

- [12] J. Roskam, *Airplane Design*. No. pt. 5 in Airplane Design, DARcorporation, 1985.
- [13] B. J. Brelje and J. R. Martins, “Development of a conceptual design model for aircraft electric propulsion with efficient gradients,” in *2018 AIAA/IEEE electric aircraft technologies symposium (EATS)*, pp. 1–25, IEEE, 2018.
- [14] G. Leishman, *Principles of Helicopter Aerodynamics with CD Extra*. Cambridge aerospace series, Cambridge University Press, 2006.
- [15] A. Brown and W. Harris, “A vehicle design and optimization model for on-demand aviation,” in *2018 AIAA/ASCE/AHS/ASC Structures, Structural Dynamics, and Materials Conference*, p. 0105, 2018.
- [16] A. Bacchini and E. Cestino, “Electric vtol configurations comparison,” *Aerospace*, vol. 6, no. 3, p. 26, 2019.
- [17] Transportup, “EHang 216.” <https://transportup.com/ehang-216/>, 2017. [Online; accessed 8-December-2021].
- [18] A. Technology, “Ehang 216 Autonomous Aerial Vehicle (AAV).” <https://www.aerospace-technology.com/projects/ehang-216-autonomous-aerial-vehicle/>, 2019. [Online; accessed 8-December-2021].
- [19] S. S. Chauhan and J. R. Martins, “Tilt-wing evtol takeoff trajectory optimization,” *Journal of Aircraft*, vol. 57, no. 1, pp. 93–112, 2020.
- [20] P. Virtanen, R. Gommers, T. E. Oliphant, M. Haberland, T. Reddy, D. Cournapeau, E. Burovski, P. Peterson, W. Weckesser, J. Bright, S. J. van der Walt, M. Brett, J. Wilson, K. J. Millman, N. Mayorov, A. R. J. Nelson, E. Jones, R. Kern, E. Larson, C. J. Carey, İ. Polat, Y. Feng, E. W. Moore, J. VanderPlas, D. Laxalde, J. Perktold, R. Cimrman, I. Henriksen, E. A. Quintero, C. R. Harris, A. M. Archibald, A. H. Ribeiro, F. Pedregosa, P. van Mulbregt, and SciPy 1.0 Contributors, “SciPy 1.0: Fundamental Algorithms for Scientific Computing in Python,” *Nature Methods*, vol. 17, pp. 261–272, 2020.
- [21] N. Wu, G. Kenway, C. A. Mader, J. Jasa, and J. R. R. A. Martins, “pyoptsparse: A python framework for large-scale constrained nonlinear optimization of sparse systems,” *Journal of Open Source Software*, vol. 5, no. 54, p. 2564, 2020.
- [22] U. Elevate, “UberAir requirement.” <https://www.uber.com/us/en/elevate/>, 2020. [Online; accessed 01-April-2022].
- [23] F. A. Administration, “14 cfr § 91.119 - minimum safe altitudes: General..” <https://www.govinfo.gov/app/details/CFR-2016-title14-vol2-CFR-2016-title14-vol2-sec91-119>, 2017. [Online; accessed 13-December-2021].

- [24] G. Palaia, K. Abu Salem, V. Cipolla, V. Binante, and D. Zanetti, “A conceptual design methodology for e-vtol aircraft for urban air mobility,” *Applied Sciences*, vol. 11, no. 22, p. 10815, 2021.

# Appendices

## A Analysis Benchmarking

The other index worth noticing is the optimizer performance during this report. Therefore, this report performed the optimizer benchmarking between SLSQP and SNOPT. Although the OpenMDAO provides the container to power the SLSQP from SciPy [20] by default, this report used both SLSQP and SNOPT optimizer from pyOptSparse [21] instead to maintain the consistency of two optimizers from the same framework. All hyperparameters are set in default for both optimizers.

### A.1 Problem Formulation

To benchmark two optimizers, we used the JobyS4 tilt-rotor configuration by fixing the cruise range, cruise speed, and battery energy density and swept the payload capacity. The detailed setup are provided as the previous JobyS4 16 table.

### A.2 Results and Discussion

Figure 21 demonstrate a benchmarking results from two optimizers. The SNOPT outperforms the SLSQP in the number of function calls for every payload sweep. More, SNOPT searches for a lower object value in the very first function calls. For example, SNOPT reaches a lower objective value in the third function calls than in the 10 to 15th functions of the SLSQP. More, as shown in Table. 17, two optimizer reaches the same optimal values. Overall, the SNOPT is better than SLSQP in terms of computation resource calls in our study.

Optimizer	Payloads(lb)	Iterations	MTOW (lb)
SLSQP	240	40	2040.069
	480	40	2614.613
	720	39	3209.042
	960	37	3830.297
	1200	39	4485.792
SNOPT	240	15	2040.069
	480	19	2614.613
	720	22	3209.042
	960	26	3830.297
	1200	19	4485.792

Table 17: Optimizer Benchmark

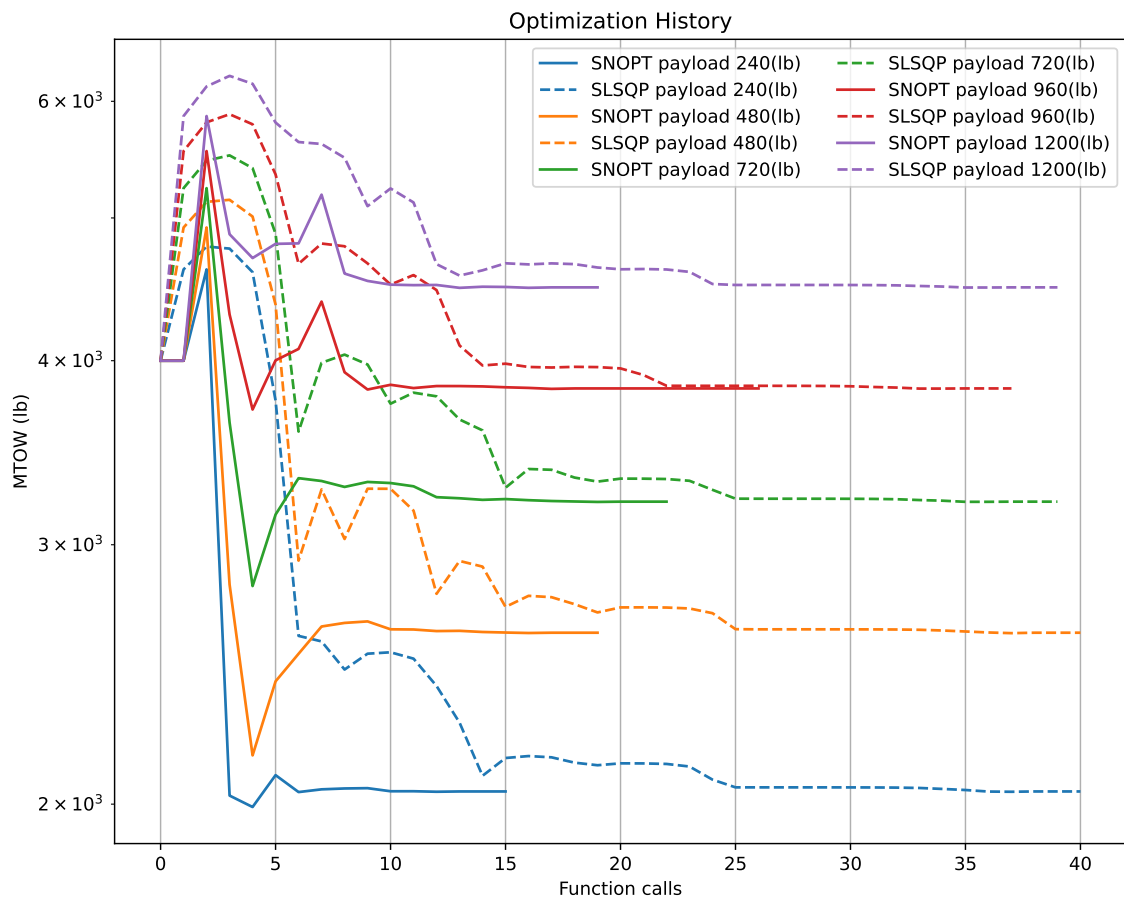


Figure 21: MTOW converge history